

Progress in Surface Modification of SnO₂ Electron Transport Layers for Stable Perovskite Solar Cells

Jue Gong, Yupeng Cui, Faming Li, and Mingzhen Liu*

The photovoltaic (PV) performance of perovskite solar cells (PSCs) has rapidly advanced in the recent years; yet, the stability issue remains one of the last-mile challenges on the road to commercialization. Charge transport layers and their interfaces with perovskites stand for critical tuning knobs that determine the device stability of PSCs. This review focuses on the effects of modification of SnO₂ electron transport layers (ETLs) on the interfacial physicochemical properties and stability of PSC devices. In detail, the intrinsic defects, surface hydroxyls, and nonuniform morphology of SnO₂ will negatively impact its interfacial physicochemical properties, thus degrading the device stability of PSCs. To tackle these existing issues, three modification approaches, such as surface morphology control, surface physicochemical modifications, and surface composite-structure design, are categorized. Lastly, future perspectives in further promoting the stability of PSCs from SnO₂ ETLs are raised based on the currently unresolved issues from both material and device levels.

1. Introduction


Since the first invention of perovskite solar cells (PSCs), its power conversion efficiency (PCE) has rapidly surged to 25.8%,^[1] with flexible PSCs also reaching a high PCE of 23.6%.^[2] However, stability of PSCs is still considerably inferior that have rendered them not able to fulfill the commercialization standards at the moment.^[3] So far, the approaches adopted to mitigate the instability issues of PSCs include enhancements of the intrinsic stability of perovskite light-harvesting materials, modification of functional layers, tailored interfacial engineering, and device encapsulations.^[4] Due to high ion mobility and intrinsic surface defects (e.g., dangling bonds, uncoordinated/undercoordinated sites) of perovskite materials,^[5] the neighboring charge transport layers that sandwich perovskite in between serve the critical roles of not only regulating but also preserving the physical/chemical integrity of perovskites. Out of the charge transport layers, hole

transport layers (HTLs) such as spiro-OMeTAD and PTAA with tailored molecular functions and interfacial properties^[6] have contributed to improved stabilities of PSCs under moisture and thermal stresses. Yet, the complementary aspects such as optical, chemical, and mechanical stabilities, as mediated by electron transport layers (ETLs), remain relatively underexplored in PSCs with n-i-p architecture.

Among the many ETLs, inorganic ETLs such as SnO₂, TiO₂, Zn₂SnO₄ have desirable properties such as high optical transparency, structural, and thermodynamic stabilities. Due to these advantages, ETL/perovskite/HTL multilayer stacks can function to effectively protect perovskite materials, constituting pivotal pathways to improve stabilities at device level in response to external stress conditions. Representing an

ETL that has retarded chemical reactivity or photocatalytic activity with perovskite materials, SnO₂ is a promising candidate for operationally stable and high-performance PSCs. Moreover, it possesses much greater electron mobility for inhibiting interfacial carrier accumulation and the consequent current-voltage (*J*-*V*) hysteresis in solar cells; the moisture-resistant, UV-tolerant natures of SnO₂ even make it potentially viable for long-term, steady-state power output of the incorporated PSCs.^[7] So far, PSCs with rigid and flexible substrates have achieved top solar-to-electricity performance with SnO₂ being the ETLs (**Figure 1**). Nonetheless, the self-doped defects at the surface of SnO₂ (such as Sn and O vacancies, surface hydroxyls, etc.) exert profound impact to the performance and stability of PSCs.^[8] In detail, hydroxyl groups (-OH) and dangling bonds on SnO₂ surface decrease the formation energy of oxygen vacancies and promote oxygen diffusion toward perovskite lattice,^[8a,b,d] while causing proton movements from the organic cations, thereby degrading the thermal stabilities of perovskite materials.^[9] As such, it can be seen that the major degradation mechanism of SnO₂-based PSCs of both the chemical properties and PV performance is mainly attributed to the defective buried interfaces between SnO₂ ETLs and perovskites, thus making the modifications at the SnO₂ surface/interfacial locations extremely crucial for stability enhancement in PSCs. To date, most article reviews of SnO₂-based PSCs mainly focus on the influence of bulk doping and surface modification of ETLs in the PV performance,^[10] with inner connections between the surface/interfacial modifications and long-term stabilities under moisture, elevated temperatures, and light irradiation conditions lacking in-depth analysis. The consolidation of this scientific building block, therefore, will inspire relevant ideas to further improvements of stability at both material and device levels.

J. Gong, Y. Cui, F. Li, M. Liu
School of Materials and Energy
University of Electronic Science and Technology of China
Chengdu 611731, P. R. China
E-mail: mingzhen.liu@uestc.edu.cn

 The ORCID identification number(s) for the author(s) of this article can be found under <https://doi.org/10.1002/smcs.202200108>.

© 2023 The Authors. Small Science published by Wiley-VCH GmbH. This is an open access article under the terms of the Creative Commons Attribution License, which permits use, distribution and reproduction in any medium, provided the original work is properly cited.

DOI: 10.1002/smcs.202200108

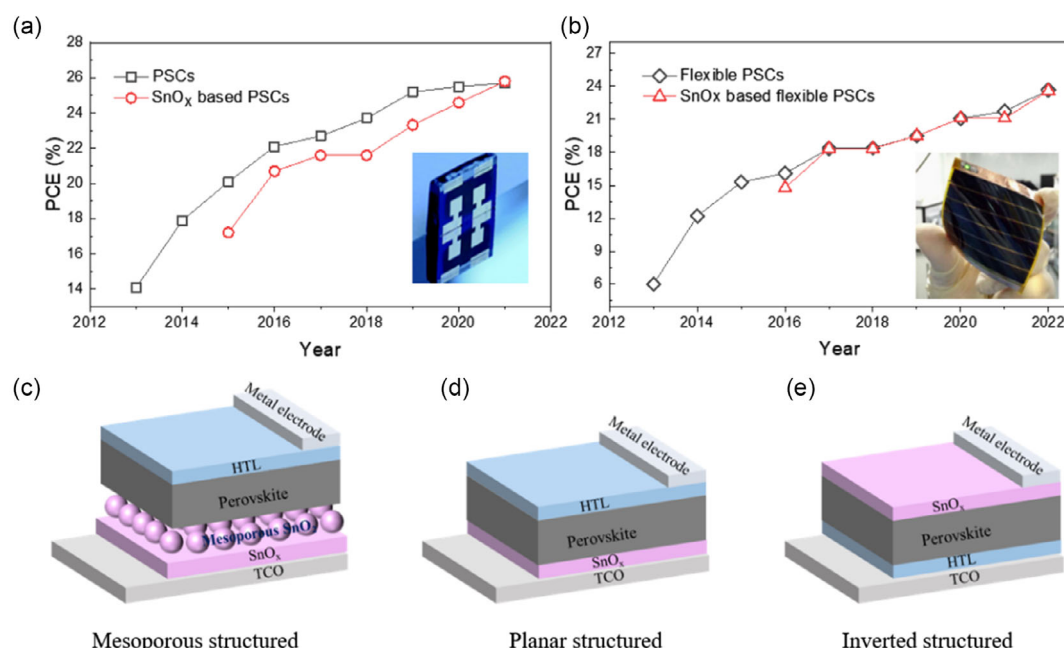


Figure 1. Research progress of PSCs based on different substrates, ETL and device structures. a) Evolution of top-performance PSCs on rigid substrates.^[1,5a,14] and b) on flexible substrates.^[2,63] Performance of devices based on SnO₂ ETLs is shown by red curves. Inset: photographs of typical rigid and flexible PSCs.^[14b,64] c–e) PSCs employing mesoporous (c), planar (d), and inverted (e) device structures.

This review focuses on surface morphology, defects, interfacial stress and energetics of SnO₂, and the corresponding effects in device stability of PSCs. Based on the underlying structure–property relationships, we further generalize and categorize three surface modification approaches—morphology control, physicochemical modifications, and composite-structure design. We first introduce the optical and electronic properties of SnO₂ ETLs in Section 2, based on which we proceed to the modification approaches of SnO₂/perovskite interfaces of PSCs in Section 3. This work will advance the understanding of the important and affecting roles of SnO₂/perovskite interfaces in stabilizing PSCs under long-term PV operation.

2. Physical Properties of SnO₂ Electron Transport Layers

Since ETLs serve the roles of electron extraction and transport in PSCs, it is desirable for them to exhibit high charge extraction potential, less charge accumulation, and less charge recombination when forming interfaces with perovskite films. In addition, ETLs are desired to possess minimum parasitic absorption so to maximize the light absorbable by perovskite active layer. In this section, we will review the properties of SnO₂ from the four aspects—photoelectric properties, energy band structures, film formation, and defect properties.

2.1. Optoelectronic Properties

2.1.1. Large Bandgap and Optical Transmittance

The optical bandgap of a semiconductor directly dictates the cut-off energy of photons that can be absorbed. SnO₂ has bandgaps

ranging from 3.60 to 4.50 eV according to different fabrication methods (Figure 2a),^[10b] which renders it transparent to most visible region when compared with other ETL materials, such as TiO₂, ZnO, and PCBM (Figure 2b,c). In detail, it is the defects, crystallinity, and/or particle sizes from different synthetic approaches that give rise to the different optical bandgaps of SnO₂, where the types and amounts of defects directly determine the relative coordination between Sn and O elements, thereby affecting the electron orbital overlap and thus the energy gap,^[11] as similar to oxygen-deficient TiO_x materials.^[12] Characteristically, SnO₂ has high transmittance (*T*) of solar spectrum above 80% within the spectral range of 400–800 nm (Figure 2b), and thus constitutes minimum parasitic absorption and ensures a full exploitation of solar irradiation by perovskite light-harvesting layers, where the relationship between *T* and absorption coefficient (α) is described as^[13]

$$T \approx e^{-\alpha t} \quad (1)$$

where *t* stands for film thickness, where SnO₂ film typically will not exceed 20–30 nm. Along with the very small α at wavelengths where light is transmissible, the transmittance by SnO₂ is typically closed to unity.

The refractive index is also an important factor affecting the light transmittance. Since SnO₂ ETLs have particularly low refractive index in the visible region, and the overall refractive index in combination with TCOs (FTO, ITO) is also much smaller than other types of ETLs.^[14,15] As such, sunlight can pass through SnO₂ ETL substrates without much loss solely due to the prolonged optical loss by refraction.

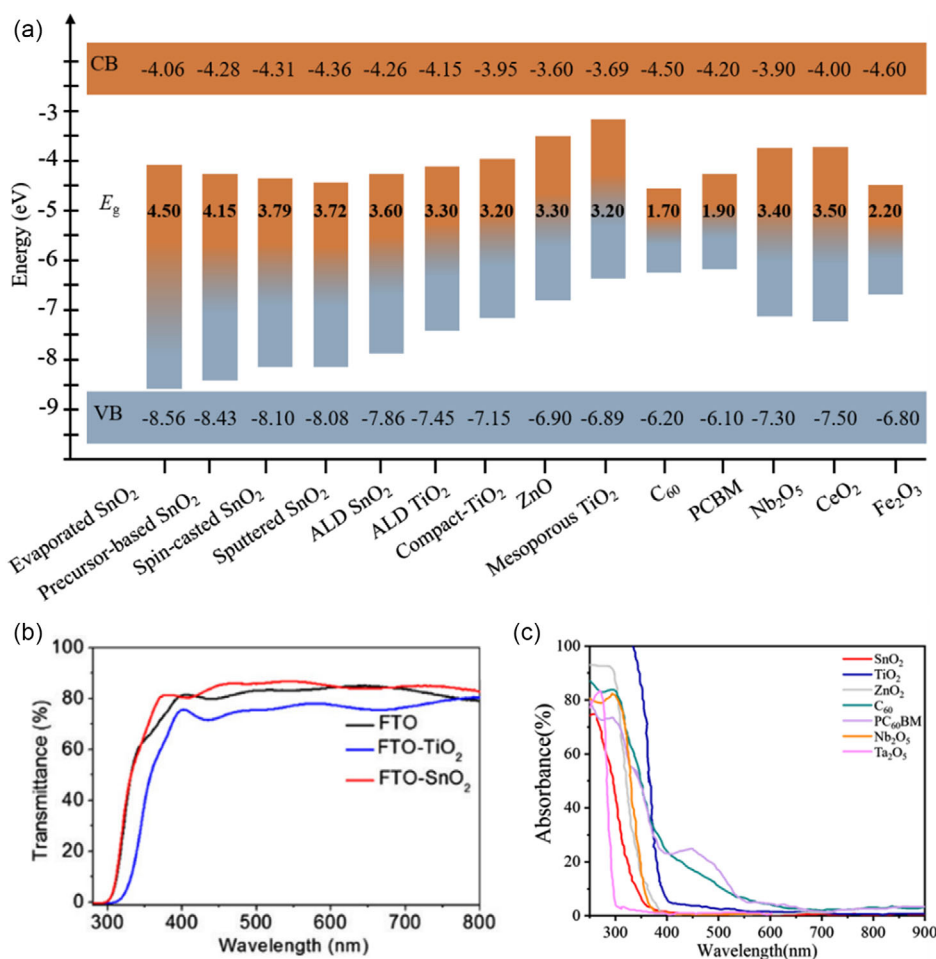


Figure 2. Comparison of optical properties of different ETLs. a) Energy band diagrams of the most commonly applied ETLs including SnO₂,^[20] TiO₂,^[20c,65] ZnO,^[66] C₆₀,^[67] PCBM,^[68] Nb₂O₅,^[69] CeO₂,^[70] and Fe₂O₃.^[71] b) Optical transmittance spectra of FTO (black), FTO-TiO₂ (blue), and FTO-SnO₂ (red) films.^[14a] c) Optical absorbance spectra of various ETLs.^[10a,72]

2.1.2. Electrical Properties

The intrinsic electrical properties of SnO₂ ETLs govern the electron transport process herein and the eventual charge collection at the conductive electrodes, as evaluated by electrical resistivity, electron density, and mobility. Pristine SnO₂ exhibits relatively low resistivity/resistance. However, obvious rise of electrical resistivity/resistance and reduction of carrier density are resulted upon Mg metal ion doping, which reach above 100 Ω -cm resistivity and 10^{15} to 10^{16} cm^{-3} carrier concentrations in the range of 2.5%–20% Mg doping, respectively, despite considerable improvement of electron mobility that falls within 10–55 $\text{cm}^2 \text{V}^{-1} \text{s}^{-1}$ (Figure 3a,b).^[16] By engineering SnO₂ ETLs for simultaneously improved mobility and conductivity, it was previously demonstrated that SnO₂ nanocrystals (NCs) exhibited boosted charge extraction after functionalized with NbO_x wrapping shells, leading to synergistically enhanced electron mobility and conductivity with 900–3000 mA cm^{-2} current density within 3–5 V electrical bias (Figure 3c,d).^[17] The increased mobility will reduce charge accumulation at the ETL/perovskite interface for remarkably suppressed hysteretic behaviors of solar cell devices. The exceptional electron

mobility and conductivity after interfacial treatments thus indicate the promising electrical performance of SnO₂ being ETLs applicable in PSCs.

2.2. Energy-Level Alignment with Perovskites

Conduction bands (CBs) of SnO₂ are notably lower in energy levels with respect to the perovskites, which renders this material a good electron extractor while effectively inhibiting hole injection from perovskite layer, thus preventing the undesirable carrier recombination. Most importantly, the CB offsets between SnO₂ and perovskites are small as compared to other ETL materials, which can therefore avoid large overpotential and V_{oc} loss while ensuring a facilitated charge transfer, as shown by the schematic band diagrams of a typical n–i–p device (Figure 4a,b).^[17] The ideal properties of SnO₂ are further exemplified by the fact that its energy band positions are highly tunable upon specific surface modification (e.g., NbO_x surface wrapping) as shown in Figure 4b. This regulative approach is highly useful as perovskites with different compositions are characteristic with Fermi

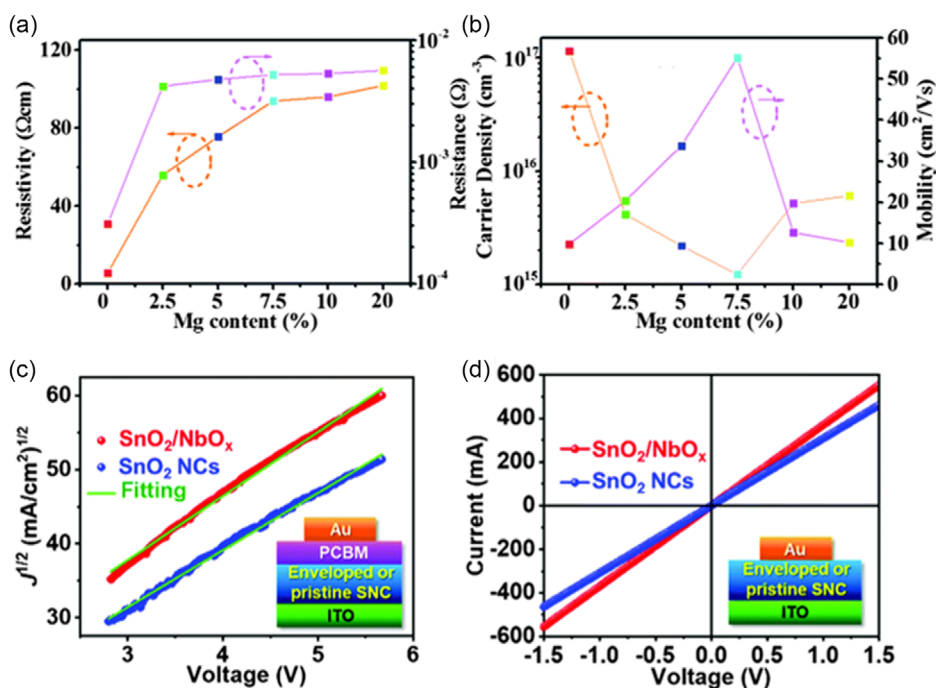


Figure 3. Electrical properties of SnO₂ ETLs with different elemental doping and functionalization. a) Electrical resistivity/resistance and b) carrier density/mobility at different Mg doping contents.^[16] a,b) Reproduced with permission.^[16] Copyright 2016, Royal Society of Chemistry. c) Mott–Gurney plots and d) I – V plots of NbO_x-enveloped SnO₂ and pristine SnO₂ NCs as ETLs.^[17] c,d) Reproduced with permission.^[17] Copyright 2021, Royal Society of Chemistry.

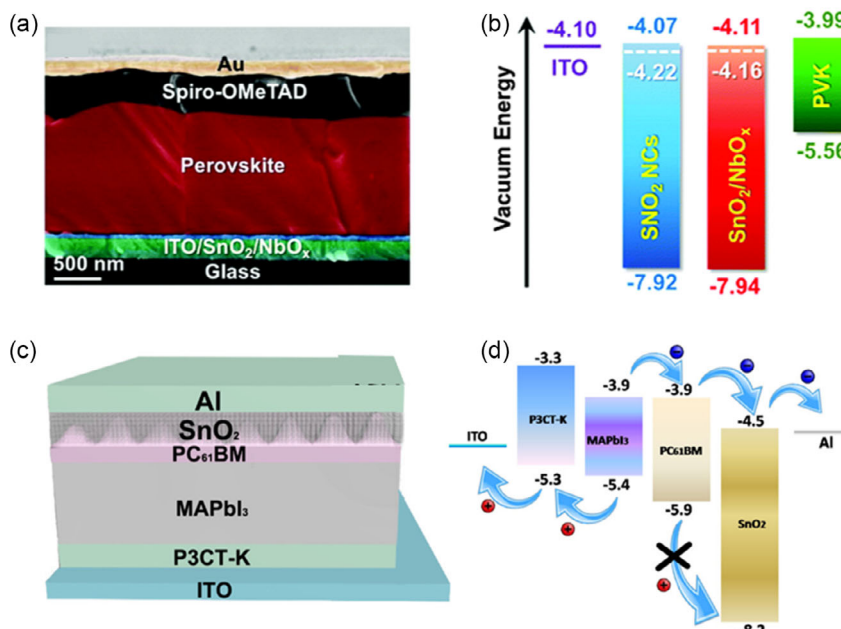


Figure 4. Device structure dependent energy-level alignments in PSCs with SnO₂ ETLs. a) Cross-section illustration of a regular n-i-p PSC and b) corresponding energy band diagrams of all functional layers.^[17] a,b) Reproduced with permission.^[17] Copyright 2021, Royal Society of Chemistry. c) Schematic depiction of inverted p-i-n PSC and d) corresponding energy band diagrams of the functional layers.^[18] c,d) Reproduced with permission.^[18] Copyright 2018, American Chemical Society.

levels, CBs, and valence bands (VBs) at different energy levels; adjusting the energy band positions of SnO₂ thus become very

necessary in realizing cascaded energetics for carrier extraction from perovskite absorbers. Moreover, the realization of SnO₂ as

ETLs is not only limited to regular n-i-p device structure, where SnO_2 ETLs can be fabricated on top of perovskites in p-i-n inverted devices through spin-casting relatively nonpolar solutions containing SnO_2 NCs (Figure 4c).^[18] Such device architecture, when composited with PCBM interlayer, can further achieve cascaded energy band alignments for minimized charge potential loss (Figure 4d). As device hysteresis is mainly influenced by the two interfaces between perovskite and charge transport layers in ETL/perovskite/HTL stacks, it is further believed that the matched energy-level alignment between SnO_2 and perovskite will also contribute to the mitigation of potential hysteretic behaviors of PSC devices.

2.3. Film Formation and Low-Temperature Processing of SnO_2 Electron Transport Layers

For the preparation of SnO_2 ETLs, various synthetic methods can be adopted such as chemical bath deposition (CBD),^[19] atomic layer deposition (ALD),^[20c,21] solution spin-coating, dip coating, slot casting, spray coating, and so on.^[22] Different synthesis approaches can result in SnO_2 films with different morphological properties that affect the stability of perovskite films and PSCs,^[23] where a summary of device stability regarding PSCs with SnO_2 ETLs with different synthesis approach is explicated in Table 1.

Among the various preparation routes, SnO_2 is most well known for its low-temperature solution processing, which does not require elevated temperature conditions for annealing to attain the benign electronic properties, whereas high temperatures between 400 and 500 °C are required to reach good crystallinity and structural integrity of TiO_2 as ETLs. Such intensive thermal conditions, however, have prevented the deployment of TiO_2 as ETLs in many device applications with heat-vulnerable substrates, such as flexible PSCs and silicon HJTs. It is exactly because of its low-temperature processing nature that renders SnO_2 ETLs energetically moderate and advantageous in flexible PSCs and large-area PSCs,^[24] making them beneficial to the low-cost, upscaled production of PSCs with pronounced application prospects. Specifically, Qi and coworkers previously fabricated large-area SnO_2 ETLs via CBD method and the scalable perovskite solar submodules with aperture area $>200\text{ cm}^2$, demonstrating a PCE $>15\%$, while the $5\text{ cm} \times 5\text{ cm}$ mini-modules using the same ETL processing exhibited a T_{80} operational stability of 1020 h;^[25] on the other hand, mini-modules with 22.8 cm^2 aperture areas based on room-temperature-sputtered SnO_2 ETLs were likewise fabricated, giving $>12\%$ device efficiency with T_{80} operational lifetime of 515 h.^[26] These results clearly demonstrate the promising potential of SnO_2 ETLs in the large-area photovoltaics with scalable sizes.

2.4. Defects in SnO_2 Electron Transport Layers

Although SnO_2 is featured with benign properties such as chemical stability, optical transparency, and low-temperature processability as elaborated earlier, surface and bulk defects nonetheless exist in SnO_2 that affect the structural and electronic properties of the interfaces and PSC devices. In detail, surface defects include oxygen vacancy (V_O),^[8a,27] hydroxyl groups ($-\text{OH}$),^[8b,d] and impurity ions, while the formation and existence

of such defects are related to the surface dangling bonds and uncoordinated/undercoordinated atoms due to the small crystallite sizes and low-crystallinity nature of SnO_2 from its low-temperature processing.^[9] Although numerous bulk defects, namely V_O , tin vacancies (V_{Sn}), tin (Sn_i)/oxygen (O_{Sn}) antisites, oxygen (O_i)/tin (Sn_i) interstitials, also exist in SnO_2 ETLs, surface defects rather play more significant roles in affecting the interfacial charge extraction from perovskite absorbers and physical quality of perovskite films deposited on top. To suppress surface defects, efforts have been carried out through surface modification methods to target the large number of dangling bonds and hydroxyl terminal defects on the surface, as detailed in later context.

3. Approaches to Improve Stability of PSCs Based on Electron Transport Layers

Stability is an important performance parameter of PSCs, which is directly related to the commercialization of PSCs.^[28] Based on the aforementioned analysis, SnO_2 has been proved to be a suitable ETL in PSCs.^[29] With various surface defects in SnO_2 hindering the optimizing of device stability in PSCs,^[30] we summarize three major pathways to improve the stability of PSCs from the perspective of SnO_2 ETLs, including surface morphological control, defect passivation, and composite-structure design, as shown in Figure 5.

3.1. Surface Morphological Control

3.1.1. Crystal Size Manipulation in SnO_2 Electron Transport Layers

Targeting the low crystallinity issue of SnO_2 ETLs as caused by the low-temperature processing, the in situ regrowth of SnO_2 NCs was reported via introducing optimum trace amounts of surface adsorbed water on FTO or ITO substrates by UV-ozone (UVO) treatments (Figure 6a).^[31] The surface water content exhibited a monotonic increment upon extended UVO treatment duration, but prolonged UVO treatment of TCO substrates led to excessive surface water that caused random agglomeration of SnO_2 crystallites, thus forming incomplete surface coverage of the underlying FTO substrates required for good PV performance of PSCs (Figure 6a).^[31] As a result, SnO_2 ETLs with the optimum morphology and greater crystallinity lead to PSC devices with greater PCE ($>20\%$) with respect to the reference and control device counterparts with less optimized SnO_2 surface morphology.^[31] The regulation of SnO_2 ETLs in affecting device performance and stability of PSCs is also manifested in the uniformity of SnO_2 nanoparticle sizes. Polymer heparin potassium (HP) was further utilized to realize homogeneous dispersion of SnO_2 colloidal nanoparticles in solution form, which directly resulted in ordered arrangement of SnO_2 NCs and perovskite films with vertically oriented grains after depositions (Figure 6b).^[32] The high-quality growth of perovskite film on top of HP-functionalized SnO_2 ETLs ultimately gave rise to exceptional device stability under continuous one-sun illumination for 1000 h with negligible performance loss, with devices fabricated on pristine SnO_2 ETLs showing more than 20% performance degradation relative to HP-treated counterparts under identical stress conditions (Figure 6c).^[32]

Table 1. Progress in the stability of perovskite solar cells based on SnO₂ ETLs with different synthetic approaches.

[Year]	ETL processing	Device structure	Stability	PCE1 ^{a)}	Ref.
				PCE2 ^{b)}	
2015	Slot-die coat SnO ₂	ITO/SnO ₂ /PVSK ^{c)} /Spiro-OMeTAD/Ag	Unencapsulated, AM1.5G, ambient air, 30 days	13.0% ≈11%	[73]
2016	SC ^{d)} -CBD SnO ₂	FTO/SnO ₂ /PVSK/Spiro-OMeTAD/Au	Unencapsulated, dry air, 90 days	20.70% >20%	[14b]
2017	Hydrothermal SnO ₂	FTO/SnO ₂ /PVSK/Spiro-OMeTAD/Au	Unencapsulated, air, RT, 500 h	18.31% 16.47%	[74]
2018	SC SnO ₂	ITO/SnO ₂ /PVSK/Spiro-OMeTAD/Au	Unencapsulated, ambient atmosphere, 2880 h	21.6% 19.87%	[14d]
2018	CBD ^{e)} SnO ₂	FTO/SnO ₂ /ZW ^{f)} /PVSK/Spiro-OMeTAD/Au	Unencapsulated, 85 °C, RH = 85%, 140 h	21.43% 19.93%	[20b]
2018	SC SnO ₂	FTO/SnO ₂ /KCl/PVSK/Spiro-OMeTAD/Au	Unencapsulated, N ₂ , 25 °C, RH = 50%–70%, 720 h	20.5% 18.45%	[75]
2019	SC SnO ₂	FTO/Ru + SnO ₂ /PVSK/Spiro-OMeTAD/Au	25 °C, 2000 h	22% 21.34%	[76]
2019	SC SnO ₂	ITO/SnO ₂ /PS ^{g)} /PVSK/PS/Spiro-OMeTAD/Au	Inner-encapsulated, 5 days	21.89% 21.23%	[53]
2019	SC SnO ₂	ITO/SnO ₂ /PVSK/Spiro-OMeTAD/Au	Unencapsulated, outdoor irradiation, 180 h/UV irradiation, 500 h	21.01% 19.75%/16.8%	[77]
2019	SC SnO ₂	ITO/SnO ₂ /PVSK/MoO ₃ /Spiro-OMeTAD/Au	Unencapsulated, RH = 40%-60%, 25 °C, dark, 1000 h	22.77% 21.63%	[7b]
2020	SC SnO ₂	ITO/In ₂ O ₃ /SnO ₂ /PVSK/Spiro-OMeTAD/Au	Unencapsulated, N ₂ , 25 °C, 80 days	23.24% 22.66%	[55]
2020	CBD SnO ₂	FTO/SnO ₂ /PVSK/Spiro-OMeTAD/Au	Unencapsulated, 85 °C, RH = 85%, 1056 h/full-sun illumination, 1620 h	24.59% 23.11%/24.09%	[14e]
2021	CBD SnO ₂	FTO/SnO ₂ /FAPbI ₃ /Spiro-OMeTAD/Au	Continuous light exposure, 500 h	25.8% 23.22%	[1]
2021	SC SnO ₂	FTO/SnO ₂ /PVSK/Spiro-OMeTAD/Au	Unencapsulated, 6–25 °C, RH = 20%–30%, air, AM1.5G, 2000 h	22.08% 20.76%	[78]
2021	SC SnO ₂	ITO/SnO ₂ /PVSK/Spiro-OMeTAD/Au	50% increase of adhesion toughness Unencapsulated, N ₂ , 4000 h	21.4% 17.12%	[49]
2021	SC SnO ₂	ITO/SnO ₂ /BGCl/PVSK/HTL/Ag	Unencapsulated, 20 °C, RH = 30%, dark, 500 h	24.4% 23.18%	[42]
2021	SC SnO ₂	FTO/SnO ₂ /PVSK/Spiro-OMeTAD/Au	Unencapsulated, N ₂ , 40 °C, one-sun, 1000 h	22.2% 18.2%	[62]
2021	SC SnO ₂	FTO/TiO ₂ /SnO ₂ /PVSK/Spiro-OMeTAD/Au	Unencapsulated, N ₂ , RH = 0%, AM1.5, 1000 h	97% of initial PCE	[79]
2021	CBD SnO ₂	FTO/SnO ₂ /PVSK/Spiro-OMeTAD/Au	Unencapsulated, 100 mW cm ⁻² , AM1.5G, 45 °C, 500 h, MPPT ^{h)}	25.4% 20.4%	[19]
2022	SC SnO ₂	ITO/SnO ₂ /FSA/ PVSK/Spiro-OMeTAD/Au	Unencapsulated, N ₂ , AM1.5G, 50-60 °C, 1000 h, MPPT	24.1% 18.08%	[80]
2022	SC SnO ₂	ITO/SnO ₂ /ADAA/PVSK/Spiro-OMeTAD/Ag	Unencapsulated, 60 °C, 1000 h	23.18% 18.78%	[52]

^{a)}PCE1: initial PCE; ^{b)}PCE2: retained PCE; ^{c)}PVSK: perovskite; ^{d)}SC: spin coating; ^{e)}CBD: chemical bath deposition; ^{f)}ZW: zwitterion; ^{g)}PS: buffer polystyrene/cap polystyrene; ^{h)}MPPT: maximum power point tracking.

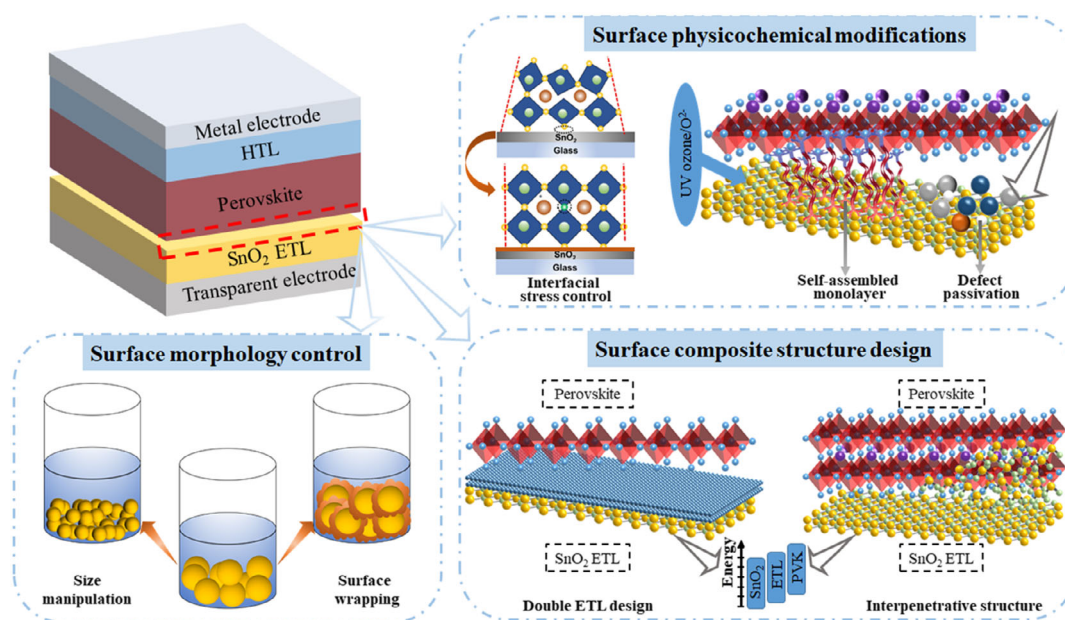


Figure 5. Schematic illustrations of the routes for improving the stability of PSCs by modifying SnO_2 ETLs. Surface modification strategies are outlined as morphological control, physicochemical modifications, and design of composite-structure ETLs. Interfacial stress schematic is reproduced with permission.^[38] Copyright 2021, Elsevier.

3.1.2. Surface Wrapping of SnO_2 Electron Transport Layers

Although size and morphological control approaches have warranted robust crystallization of perovskite layers on top and stable operational stability of PSC devices, interfacial energetics and surface defects still await a synergetic manipulation for maximally enhanced device performance and stability. It was found that by wrapping SnO_2 NCs with amorphous NbO_x exterior layer (Figure 7a), the NbO_x -enveloped ETL exhibited optimized energy-level alignment with perovskite with smaller charge potential offset (Figure 7b), thereby facilitating carrier extracting while minimizing V_{oc} loss.^[17] Most importantly, unencapsulated PSC devices based on NbO_x -enveloped SnO_2 NCs as ETLs exhibited considerably improved device stability under thermal stress conditions (Figure 7c).^[17] The beneficial effects of SnO_2 surface wrapping are further corroborated by similar works. Moreover, SnO_2 NCs as capped with polyacrylamide (PAM) also gave rise to larger perovskite grain size and matched energy-level alignment with the perovskite layer on top (Figure 7d,e).^[33] As a result of the ETL modification, unencapsulated solar cell devices based on PAM-functionalized SnO_2 ETLs exhibit much enduring performance under 50% relative humidity (RH) by retaining more than 90% of the original efficiency, in contrast with the control devices based on pristine SnO_2 ETLs (Figure 7f).^[33]

3.1.3. Micro- and Nanostructure Designs in SnO_2 Electron Transport Layers

Although SnO_2 ETLs possess low-temperature processability as mentioned in Section 2.3, it can nevertheless be synthesized at high temperatures through hydrothermal methods. Most importantly, in combined with acidic aqueous environment,

nanostructured SnO_2 such as nanorod, nanotube, and nanofiber arrays can be grown.^[34] Such nanostructured SnO_2 ETLs possessed controllable area densities or wall thicknesses with well-defined, and upright structural orientations. When applied in PSCs, devices based on these nanostructured ETLs showed much enhanced PV performance and long-term stability as compared to the compact ETL-based control PSCs. Similarly, as aggregated from constituent nanocrystals, SnO_2 with microsphere shapes with large specific surface areas, high crystallinity, and tunable sizes can be formed,^[35] resulting in considerable PV performance in PSCs.

3.1.4. Effects of Posttreatments on the Surface Morphology of SnO_2 Electron Transport Layers

In contrast with the abovementioned approaches that all adopt in situ control over the morphology of SnO_2 ETLs, posttreatments can also effectively modify the surface morphology of SnO_2 ETLs. In specific, it was reported that the as-synthesized SnO_2 ETLs react with ammonium (NH_3) that triggered crystal fusion at the surface;^[36] this surface microstructural modification led to optimized interfacial contact with perovskite layer on top by creating nucleation sites. Based on enhanced interfacial charge transport and suppressed structural defects, PSCs based on the NH_3 -treated SnO_2 ETLs showed improved device stability with 86% retained performance after 60 days of aging at room temperature in 40%–50% RH.^[36] Likewise, posttreatment etching of SnO_2 ETLs in NH_4F aqueous solution gave much smoother surface morphology with greater SnO_2 coverage^[37] and eventually resulted in higher device PCE and fill factor than the PSCs with pristine SnO_2 ETLs. Importantly, PSCs based on $\text{SnO}_2/\text{NH}_4\text{F}$ ETLs showed >80% retention of initial performance,

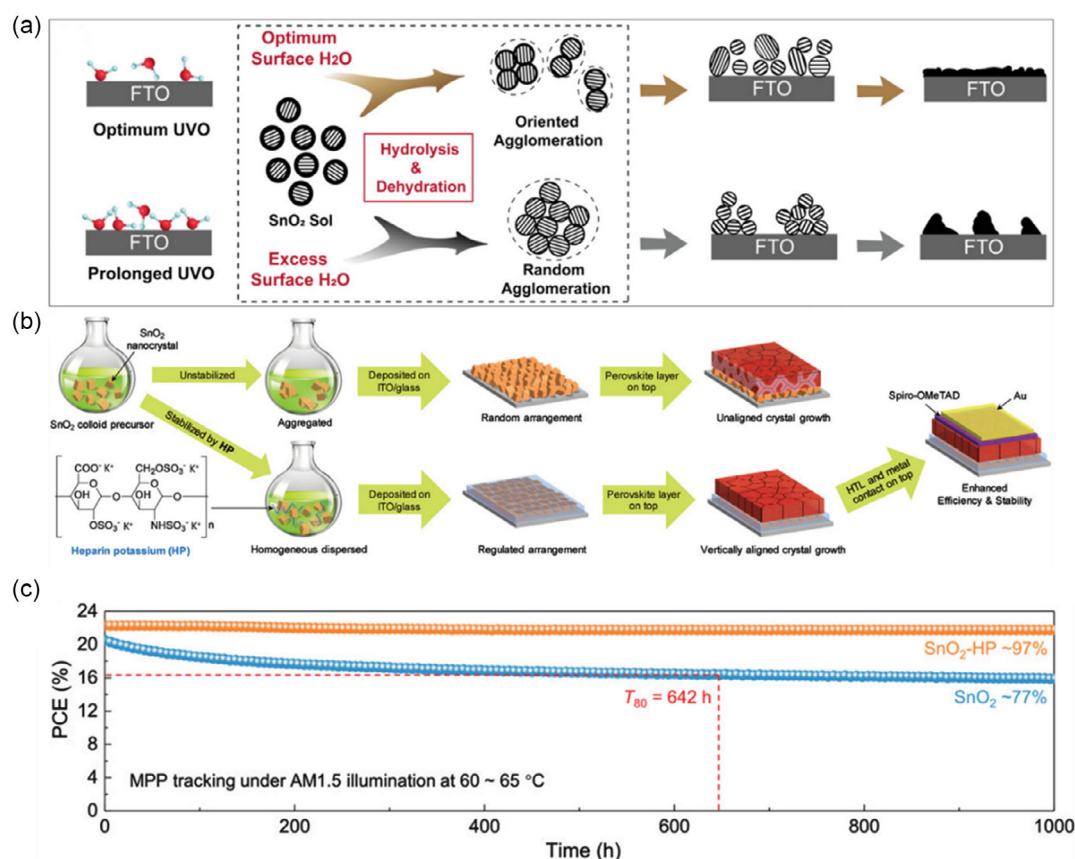


Figure 6. Particle and morphological control of SnO₂ ETLs. a) Schematic depiction of H₂O pretreatment through UVO for subsequent deposition of ETLs with different SnO₂ particle sizes.^[31] Reproduced with permission.^[31] Copyright 2019, Wiley-VCH. b) Processing scheme of polymer-regulated SnO₂ NCs for ETLs of high-performance PSCs.^[32] c) MPP tracking of solar cell devices based on pristine and polymer-regulated SnO₂ ETLs under continuous one-sun illumination for 1000 h.^[32] b,c) Reproduced with permission.^[32] Copyright 2020, Wiley-VCH.

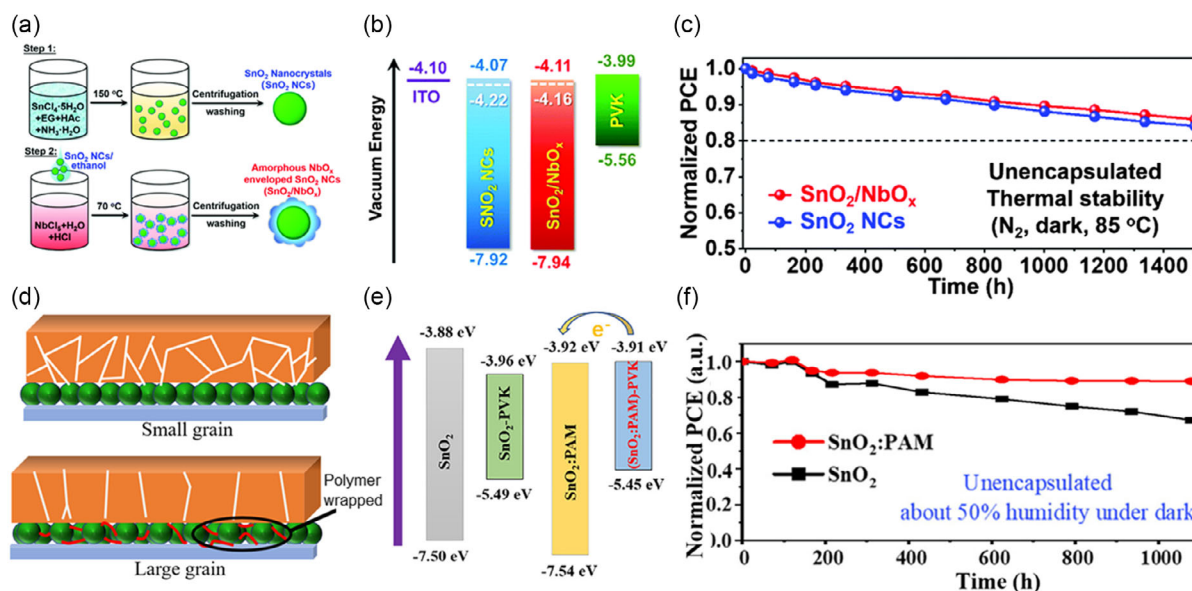


Figure 7. Surface wrapping and functionalizing in SnO₂ ETLs for stable PSCs. a) Synthesis scheme, b) energy-level alignment, and c) thermal stability of devices based on pristine and NbO_x-wrapped SnO₂ NCs as ETLs.^[17] a–c) Reproduced with permission.^[17] Copyright 2021, The Royal Society of Chemistry. d) Schematic illustration, e) energy band diagrams and f) corresponding device stability of polymer-functionalized SnO₂ as ETLs, for comparison with nontreated SnO₂ ETLs.^[33] d–f) Reproduced with permission.^[33] Copyright 2022, American Chemical Society.

outperforming the <60% retention on devices with pure SnO₂ ETL after 30 days of aging in ambient air with 40% RH.^[37]

3.2. Surface Physicochemical Modifications

Defects of SnO₂ thin films greatly influence their electronic properties and the physical quality of perovskite crystallization atop, and the interfaces with perovskite therefore represent active sites that regulate the performance of PSCs.^[38,39] Passivation of SnO₂ surface defects commonly adopted surface modification methods including UV/UVO, ionic compounds, carbon derivatives, acids, self-assembled monolayers (SAM), fullerene derivatives, macromolecular polymers, where a comprehensive summary of device performance and stability of PSCs with surface defect passivation treatments is given in Table 2.

3.2.1. Passivating Oxygen Vacancies at SnO₂ Surface

Among the many passivation strategies, UVO represents one that can effectively remove oxygen vacancies through decomposing hydroxyls, surface dangling bonds, and other organic contaminants from metal oxide surfaces, thereby eliminating carrier recombination centers for robust interfacial stability. The effect of UVO treatment on operation stability of perovskite light-emitting diodes was previously studied (Figure 8a), and found that the luminance of the fabricated light-emitting devices

exhibited notably enhanced stability with UVO treatment on the SnO₂ ETLs (Figure 8b).^[40] With a more in-depth investigation, it was confirmed that the reduced oxygen vacancies at SnO₂ surface as functionalized by UVO treatment contribute to a great crystallization quality of perovskite film on top (Figure 8c,d).^[41] Furthermore, physicochemical relationship between SnO₂'s surface oxygen vacancies and thermal instability of perovskite thin films was further revealed, as indicated by plasma treatments in different atmospheric gases and a thermal stress at 85 °C for 120 h (Figure 8e).^[9] As a result of the oxygen vacancy elimination, PSCs based on O₂-plasma surface treatment exhibited the greatest stability under imposed thermal stress (Figure 8f).^[9]

In terms of chemical passivation of SnO₂ surface defects, passivation molecules at the SnO₂/perovskite interfaces should have both electronegative and electropositive functional groups to passivate the undercoordinated Sn (electron-poor) and O (electron-rich) atoms. After passivation, surface dangling bonds associated with these undercoordinated surface atoms as recombination centers are eliminated due to the formation of new chemical bonds.^[10a] To meet such requirements of surface passivation, zwitterions are the ideal choices as passivation agents. Zwitterion—3-(1-pyridinio)-1-propanesulfonate was previously used to modify SnO₂ ETL to improve the thermal stability of solar cell device.^[20b] The zwitterionic compound led to the formation of interfacial dipole (Figure 9a) and a changed work function of SnO₂ ETL, thus preventing reversed electron transfer and inhibiting charge recombination. Furthermore, due to the positively charged ions,

Table 2. Various approaches for improving the stability of PSCs by surface defect passivation of SnO₂ ETLs.

Passivation	Device architecture	Stability	Retained PCE	Ref.
UV	ITO/SnO ₂ /PVSK ^{a)} /PEDOT/MoO ₃ /Ag	Unencapsulated, 1 sun, N ₂ , 10 h, MPPT ^{b)} , interface stability	80%	[81]
SVA ^{c)}	ITO/SnO ₂ /PVSK/Spiro-OMeTAD/Ag	Unencapsulated, ambient air, 700 h	≈90%	[73]
PS ^{d)}	ITO/SnO ₂ /Buffer ps/PVSK/Cap ps/Spiro-OMeTAD/Au	Inner encapsulated, 5 days	97%	[53]
Zwitterionic	FTO/Zw-SnO ₂ /PVSK/HTL/Au	Unencapsulated, 85 °C, RH = 85%, 140 h	93%	[20b]
CIMPI ^{e)}	ITO/SnO ₂ /PVSK/Spiro-OMeTAD/Au	Unencapsulated, outdoor, 180 h; 365 nm UV, 100 mW cm ⁻² , 2500 h; Unencapsulated, AM1.5G, N ₂ , MPPT, 500 h	94% 82%	[77]
BGCI ^{f)}	ITO/SnO ₂ /BGCI/PVSK/PEAI/MoO ₃ /Spiro/Ag	Unencapsulated, 20 °C, RH = 30%, dark, 500 h	95%	[42]
FI-SnO ₂ ^{g)}	FTO/SnO ₂ /PVSK/Spiro-OMeTAD/Au	Unencapsulated, N ₂ , 40 °C, 1 sun, 1000 h, mechanically robust	82%	[62]
NbOx	ITO/SnO ₂ /NbO _x /PVSK/Spiro-OMeTAD/Au	Unencapsulated, N ₂ , dark, RT, 2000 h; Unencapsulated, N ₂ , 1 sun, 1000 h	95% 85%	[17]
KCl	FTO/SnO ₂ /PVSK//Spiro-OMeTAD/Au	Unencapsulated, N ₂ , 25 °C, RH = 50%–70%, 720 h	90%	[75]
ImAcH-Cl ^{h)}	ITO/SnO ₂ /ImAcHCl/PVSK/Spiro-OMeTAD/Au	Unencapsulated, RT, dark, RH = 40%–60%, 35 days	94%	[82]
ADAA ⁱ⁾	ITO/SnO ₂ /ADAA/PVSK/Spiro-OMeTAD/Au	Unencapsulated, RH = 20%–30%, dark, 1200 h; unencapsulated, 60 °C, dark, N ₂ , 1000 h; unencapsulated, 1 sun, RT, 1000 h	92.4% 81% 52%	[52]
KPF ₆	ITO/SnO ₂ /KPF ₆ /PVSK/Spiro-OMeTAD/Au	Unencapsulated, RH = 15%–20%, RT, dark, 1440 h; unencapsulated, N ₂ , 60 °C, dark, 960 h; unencapsulated, 1 sun, RT, N ₂ , 960 h	94.7% 80.1% 57.2%	[38]
FSA ^{j)}	ITO/SnO ₂ /FSA/FAPbI ₃ /Spiro-OMeTAD/Au	Unencapsulated, N ₂ , AM1.5G, 50–60 °C, MPPT, 1000 h	85%	[80]
I-SAM	ITO/SnO ₂ /I-SAM/PVSK/HTL/Au	Unencapsulated, 1-sun continuous illumination, N ₂ , RT, MPPT, 3921 h	80%	[49]

^{a)}PVSK: perovskite; ^{b)}MPPT: maximum power point tracking; ^{c)}SVA: solvent vapor annealing; ^{d)}PS: polystyrene; ^{e)}CIMPI: chlorine-rich mixed-halide perovskite interlayer; ^{f)}BGCI: biguanide hydrochloride; ^{g)}FI-SnO₂:FAI-incorporated SnO₂; ^{h)}ImAcH-Cl: 4-imidazoleacetic acid hydrochloride; ⁱ⁾ADAA: 1-adamantaneacetic acid; ^{j)}FSA: formamidine sulfonic acid.

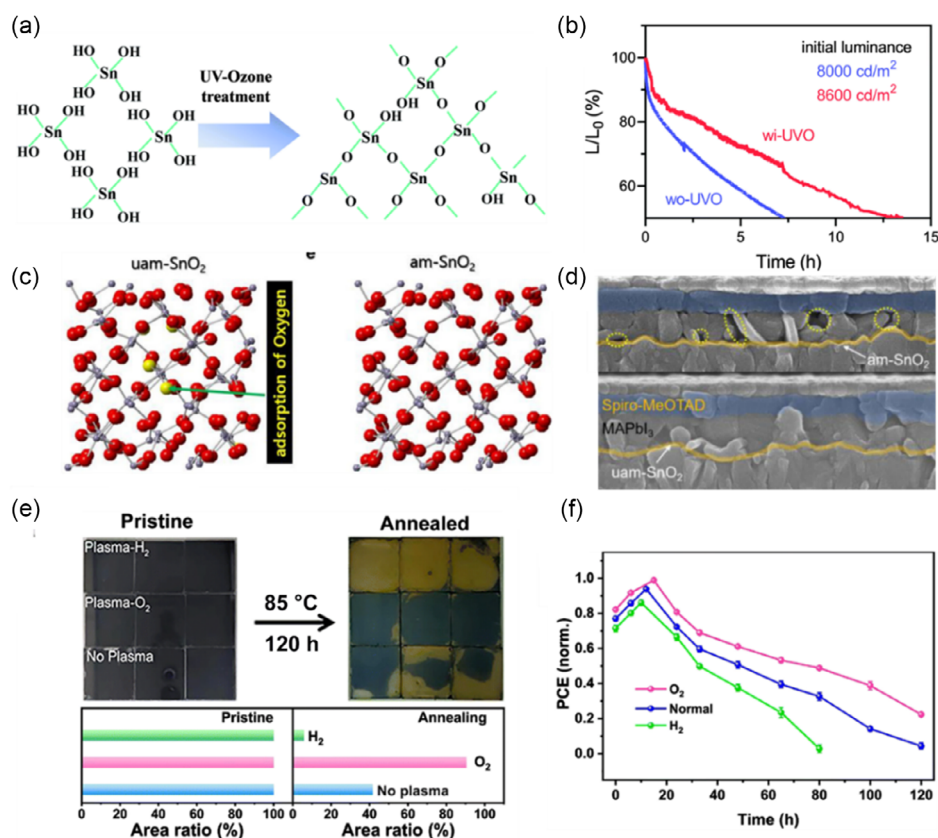


Figure 8. Effects of surface defect annihilation in the device performance stability. a) UVO treatment for elimination of surface hydroxyls from SnO₂ ETLs.^[40] b) Stability of light-emitting devices with or without UVO treatment.^[40] a,b) Reproduced with permission.^[40] Copyright 2021, The Royal Society of Chemistry. c) Oxygen vacancy healing by UVO treatment.^[41] d) Cross-section SEM images of perovskite/SnO₂ without (upper) and with (bottom) UVO treatment.^[41] c,d) Reproduced with permission.^[41] Copyright 2020, Elsevier. e) Photographs of SnO₂-based perovskite films with different plasma treatments before and after thermal stress.^[9] f) Device stability with SnO₂ ETLs with plasma treatments in different atmospheric conditions after different thermal stress durations.^[9] e,f) Reproduced with permission.^[9] Copyright 2022, The Royal Society of Chemistry.

zwitterion passivated Pb/I antisite defects within perovskite lattice, thereby improving thermal stabilities of perovskite films (Figure 9b) and solar cell devices under double 85 test conditions (Figure 9c).^[20b] Likewise, bifunctional ionic additive—biguanide hydrochloride (BGCl) was applied at the interface of SnO₂/perovskite to form hydrogen bonding with halides at perovskite's bottom surface while forming electrostatic and Lewis coordination with the underlying SnO₂ ETL (Figure 9d), thus passivating the interfacial defects in a holistic format. As a result of the interface modifications, BGCl-treated solar cell devices exhibit a remarkable 24.4% device efficiency. Without encapsulation, BGCl-treated devices only sustained less than 5% loss of efficiency after 500 h of aging under ambient conditions with 30% RH at 20 °C (Figure 9e).^[42]

The effects of interfacial passivator in defect suppression can be further tuned by tailoring the number and position of functional groups on organic ring structures. It was previously demonstrated that chlorobenzene sulfonic potassium (Cl-BSAK) salts can fill oxygen vacancies on the SnO₂ surface via coordination bonds between Cl and Sn (Figure 10a).^[43] In contrast, first-principles density functional theory (DFT) calculations revealed the inclined interaction between sulfonate group and perovskite,

where most stable configuration was achieved by 3Cl-BSAK on perovskite surface (Figure 10b).^[43] Furthermore, it was found that 3Cl-BSAK with the greatest number of Cl was conducive to the greatest performance enhancement of PSCs, in which unencapsulated devices based on 3Cl-BSAK treatment exhibited more than 95% retention of original efficiency after 2400 h of aging in dry environment and 80% retention of initial performance after 800 h of thermal stress at 80 °C (Figure 10c).^[43]

Due to the large deformation of substrates during thermal annealing, flexible PSCs suffer from large interfacial residual stress issues that largely plague the operational stabilities of PSCs under bending or illumination conditions. From mechanistic perspective, the large interfacial residual stress usually stems from interfacial defects or discrepant thermal expansivity between ETLs and perovskites.^[44] Therefore, it is imperative to develop modification strategies that can achieve defect passivation of SnO₂ ETLs to resolve the instability issues in flexible PSCs. Non-fullerene acceptor molecule Y6 (fused dithienothiophen[3,2-b]-pyrrolobenzothiadiazole derivative) was previously used as a buffer layer in SnO₂ ETLs (Figure 11a).^[45] The Y6 treatment greatly resulted in relaxed interfacial stress, and the as-fabricated flexible PSCs showed evidently improved mechanical

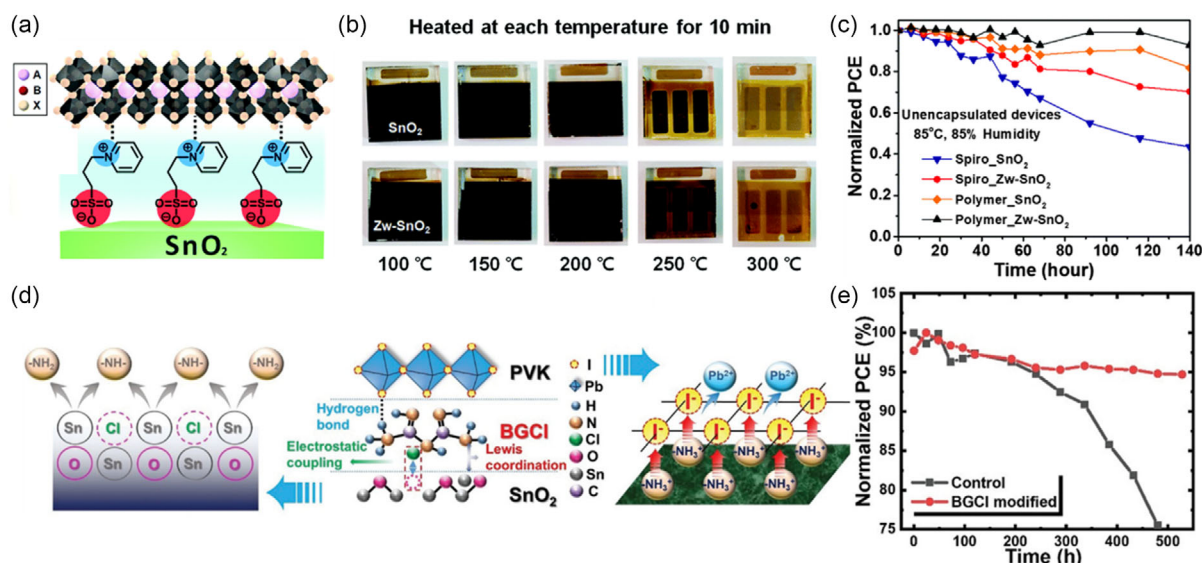


Figure 9. Surface defect passivation of SnO₂ by dipolar zwitterions and organic halide for stability improvements. a) Schematic depiction of zwitterion passivation of SnO₂ surface defects.^[20b] b) Photographs of perovskite films under thermal stress on different SnO₂ surface treatments.^[20b] c) Device stability of unencapsulated PSCs based on different SnO₂ treatment and HTLs.^[20b] a–c) Reproduced with permission.^[20b] Copyright 2018, Royal Society of Chemistry. d) Schematic illustration and interlayer chemistry of BGCI functionalization at the SnO₂/perovskite interface.^[42] e) Device stability of PSCs based on pristine and BGCI-treated SnO₂ ETLs.^[42] d,e) Reproduced with permission.^[42] Copyright 2022, Wiley-VCH GmbH.

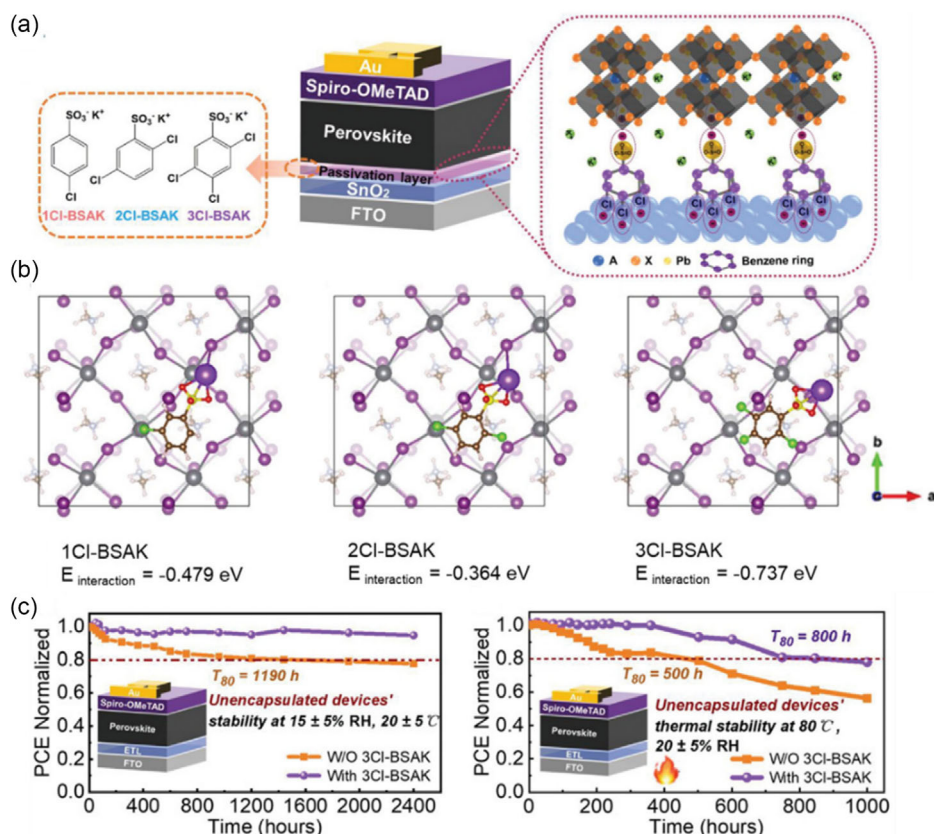


Figure 10. a) Device and mechanistic schematics of chlorobenzene sulfonic potassium salts in passivating the buried interfaces of PSCs.^[43] b) Theoretical models of perovskite-BSAK interactions used in first-principles DFT calculations.^[43] c) Stability tests of unencapsulated devices at room temperatures (left) and elevated temperature conditions (right).^[43] a–c) Reproduced with permission.^[43] Copyright 2022, Wiley-VCH GmbH.

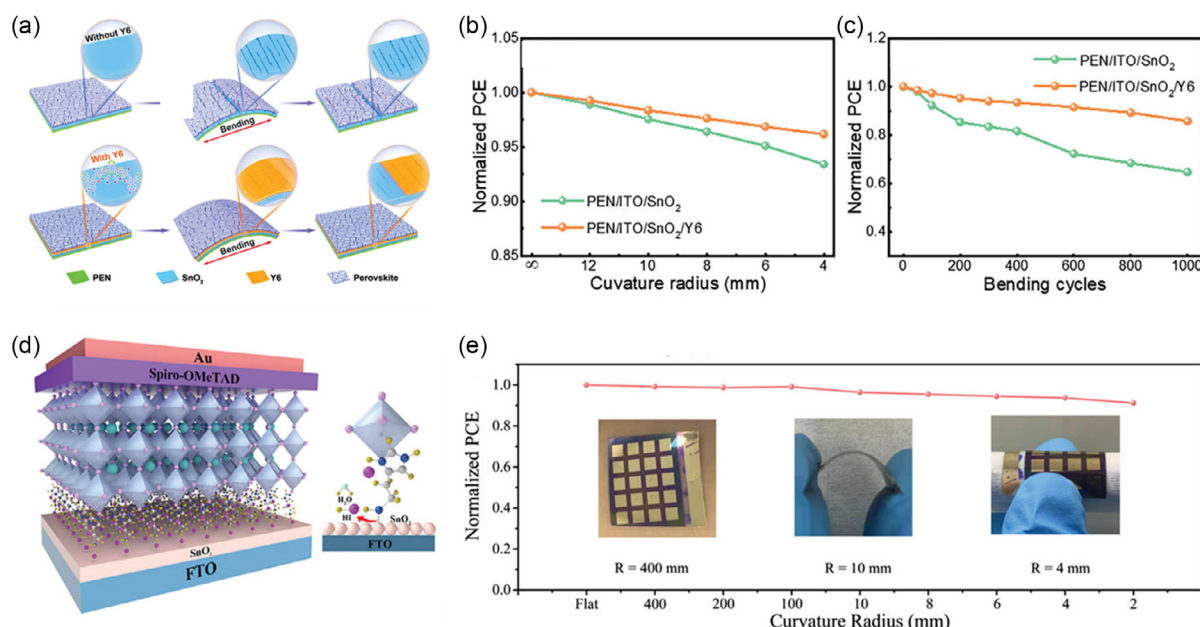


Figure 11. Additive-functionalized SnO₂ ETLs for stable flexible PSCs. a) Schematic illustration of Y6 functionalization in SnO₂ for mechanically durable flexible PSCs.^[45] b,c) Device stability of flexible PSCs based on pristine and Y6-treated SnO₂ ETLs at different bending curvatures (b) and at 8-mm radius for different cycles (c).^[45] a–c) Reproduced with permission.^[45] Copyright 2022, Wiley-VCH GmbH. d) Schematic illustration of PSC device with HADI treatment on the SnO₂ ETLs.^[46] e) Stability test of flexible PSCs at different bending curvature radius. Inset: photographs of flexible PSCs under bending conditions.^[46] d,e) Reproduced with permission.^[46] Copyright 2022, Wiley-VCH.

durability at different bending radius and bending cycles (Figure 11b,c).^[45] Similarly, multifunctional histamine diiodide (HADI) additive was applied to cure the defects at the buried interface of SnO₂/perovskite (Figure 11d), forming interlayer bridging structures that refine charge transfer and energy band alignments.^[46] Consequently, flexible PSCs with HADI-treated SnO₂ ETLs displayed exceptional mechanical stability upon different bending curvature radii (Figure 11e), thus suggesting the transferable efficacy of multifunctional ionic additives in improving both rigid-based and flexible PSCs.^[46]

3.2.2. Inhibiting Surface Hydroxyls of SnO₂ Electron Transport Layers

As pointed out in previous context, surface hydroxyls of SnO₂ ETLs play a significant role in causing the instabilities of perovskite layers and solar cell devices, where the existence of hydroxyls not only induce intrinsic defects of SnO₂ ETLs but also negatively impact the buried interface between SnO₂ and perovskites. To mitigate the defective interface as a whole, researchers have come up with novel strategies that used SAMs to optimize the interfaces.^[47] A typical SAM molecule is structurally composed of three parts: anchoring group, interterminal group, and terminal group (Figure 12a).^[48] To react with surface hydroxyls, anchoring groups of SAMs (typically phosphonic, hydroxyls, and carboxylic acid groups) first bind with the hydroxyls at SnO₂ surface through condensation, whereas terminal groups of SAMs can then have the potentials to fill the halide vacancies of perovskite bottom surface, thus modifying the buried interface. A concept of “molecular glue” at the SnO₂/perovskite

interface was previously proposed by adopting 3-iodopropyl trimethoxysilane (Si(OCH₃)₃CH₂)₃I, I-SAM) as molecular treatment to enhance adhesion toughness between SnO₂ and perovskite, as shown in Figure 12b.^[49] The mechanical strength of I-SAM-treated SnO₂/perovskite interface could be further illustrated by the much less voids/cracks formed upon perovskite film delamination from the substrate (Figure 12d), as compared to the fractured perovskite film without SAM functionalization with rampant morphological defects (Figure 12c).^[49] The increased interfacial mechanical stability resulted in profound operational stabilities of I-SAM-treated PSCs under continuous illumination, in comparison with the device counterparts treated with H-terminated SAM (H-SAM) and control devices without SAM treatments (Figure 12e).^[49] The observed device stability brought by interfacial I-SAM again corroborates the importance of multifunctional treatments that not only chemically passivate SnO₂ ETLs but also modify the bottom surfaces of perovskite layers.

Particularly, the application of SAMs at the ETL/perovskite interface finds the best application scenario in flexible PSCs. As demonstrated in the above context, SAM can formidably enhance interfacial toughness of SnO₂/perovskite junction. And when applied in flexible PSCs, it was shown that their performance stability under bending stress was greatly improved (Figure 12f, left).^[50] In detail, SAM-functionalized flexible PSCs with optimized upper surface LD structural engineering yielded 88% retention of original performance after 10 000 cycles at a bending radius of 5 mm, while showing T₉₀ operational lifetime of 1000 h under continuous one-sun illumination, which remarkably outperformed the flexible PSC counterparts with untreated SnO₂/perovskite interfaces that exhibited T₈₀ lifetime

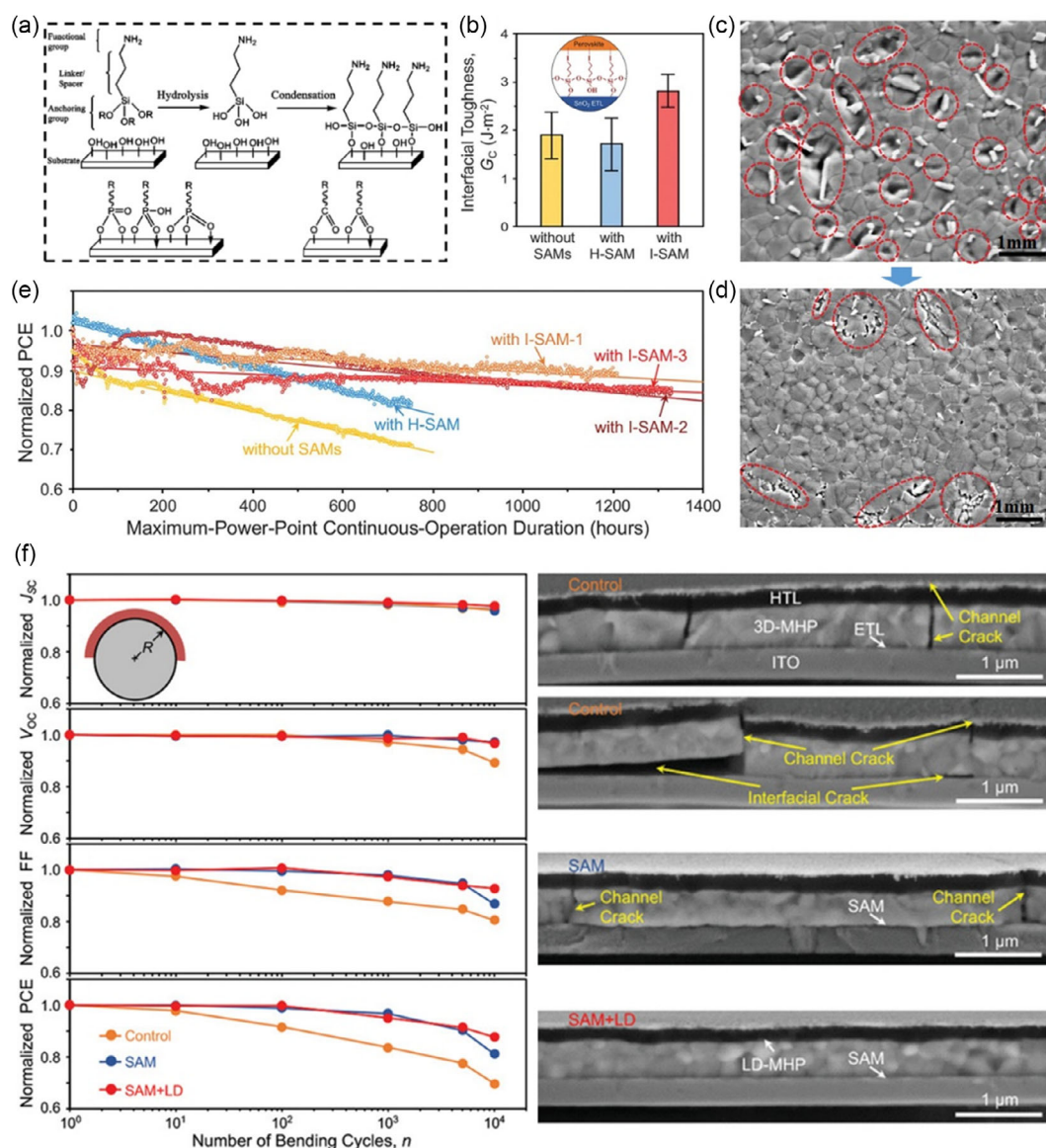


Figure 12. SAMs in achieving surface defect passivation of SnO₂ ETL. a) Schematic diagram of synthetic process of SAMs.^[48] Reproduced with permission.^[48] Copyright 2020, Wiley-VCH. b) Mechanical toughness of SnO₂/perovskite interfaces without and with SAMs functionalization. c, d) SEM images of perovskite surfaces as delaminated from substrates without SAM treatment (c) and with iodine-terminated SAM (d). e) Operational stability of PSCs without and with SAM treatments under continuous one-sun illumination and maximum power point (MPP) tracking.^[49] b–e) Reproduced with permission.^[49] Copyright 2021, American Association for the Advancement of Science. f) Mechanical reliability of flexible PSCs under bending stress. Left: device stability as function of bending cycle with at a radius of 5 mm. Right: cross-section SEM images of flexible devices with and without SAM at the SnO₂/perovskite interface after the 10 000-cycle bending. Reproduced with permission.^[50] Copyright 2022, Wiley-VCH.

of only 600 h, currently topping the operational performance stability among all flexible PSCs reported.^[50] The corresponding cross-section morphology of untreated flexible PSCs showed omnipresent channel and interfacial cracks that were distributed after the bending stress, whereas SAM + LD devices were free of such morphological degradation (Figure 12f, right). By comparing the above-mentioned modifications in flexible PSCs, one can infer on the much greater efficacy of interfacial SAMs in curing the surface defects of SnO₂, and thus the enhancements in mechanical and operational stabilities of flexible PSCs than just the ionic additives.

3.2.3. Enhancing Surface Adhesion of SnO₂ Electron Transport Layers

Although we have shown that extensive efforts have successfully passivated surface defects in SnO₂ ETLs, the stability of PSCs nevertheless also depends on the residual stress sustained by perovskite layers.^[51] From fundamental perspectives, residual stress at the interface arises from discrepant thermal expansivity between ETL and perovskite film after thermal annealing.^[51c] Thermally induced tensile stress in the perovskite film weakens chemical bonds, reduces the formation energy of defects, and

reduces the activation energy of ion migration, which therefore accelerates the degradation of perovskite film under illumination and electrical bias conditions.^[9] In this regard, adamantane derivative molecules (AD, ADCA, and ADAA) containing carbonyl (C = O) functional groups were used to modify the SnO₂ ETL/perovskite contact for passivating the interfacial defects, while releasing the residual stress therein. The passivation molecule coordinates with the oxygen vacancy defects in SnO₂ while simultaneously binding with the undercoordinated Pb in perovskite (Figure 13a).^[52] In contrast, functionalized SnO₂ ETLs with the molecular treatments led to notable relief of residual stress in perovskite thin films (Figure 13b).^[52] Among the three molecular modifiers, theoretical modeling further confirms the vital roles of steric hindrance in affecting the interfacial stress relaxation and thus the integral stability of PSC devices (Figure 13c), where the stabilizing effects exhibit an order of ADAA > ADCA > AD on unencapsulated devices under thermal stress, continuous one-sun illumination and ambient conditions (Figure 13d).^[52] The results indicate that unlike chemical modification of SnO₂/perovskite buried interface, the ordered arrangement of passivation molecules according to their mutual steric hindrance is also an important factor for consideration in regulating interfacial residual stress.

Instead of regulating the interfacial residual stress through organic molecule's steric hindrance, polystyrene (PS) was introduced into PSCs as a buffer layer between SnO₂ ETL and perovskite film, as shown in Figure 14a.^[53] Due to the soft polymer

nature, PS formed continuous film and properly alleviated the interfacial strain between SnO₂ ETL and perovskite film by reducing the modulus mismatch, thereby improving the structural integrity of perovskite lattice. Consequently, PSCs with PS interfacial treatment showed greatly enhanced operation stability under continual one-sun illumination in ambient atmosphere, as well as illumination–dark cycle stability for more than 100 h (Figure 14b).^[53] Instead of adopting the mindset of interfacial buffer layer, an idea of implanting volatile organic additive—ammonium formate (NH₄COOH) within SnO₂ ETL was previously devised, where NH₄COOH vaporized during perovskite film annealing to realize an in situ and integral modification of SnO₂ ETL, perovskite layer and their interface (Figure 14c), thus achieving a formidably released interfacial stress (Figure 14d).^[44] Most profoundly, perovskite films on flexible substrates functionalized with such preburied NH₄COOH additive exhibited minimum morphological degradation (Figure 14f), in contrast to the untreated films that showed obvious cracks and delamination after 4000 cycles of mechanical bending (Figure 14e), much alike to the strengthening effects of I-SAM on the interfacial toughness as discussed above.^[44] However, differentiation needs to be made between the treatments on SnO₂ ETLs by halide-containing molecules (e.g., I-SAM) and the ammonium-based volatile additives (e.g., NH₄COOH) as owing to their different working mechanisms of interfacial modifications. In specific, previous research revealed that light-induced performance degradation of PSCs mainly arose from the generation of iodide

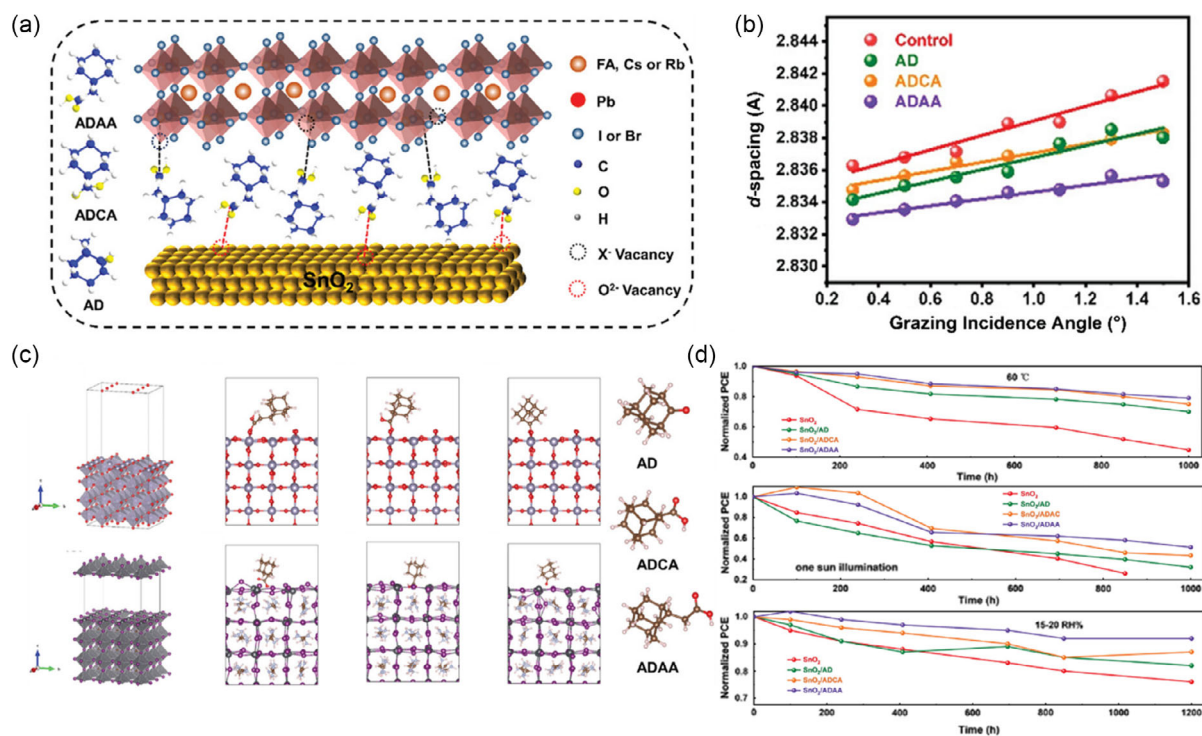


Figure 13. Strain relaxation of SnO₂/perovskite interfaces for stable device performance. a) Schematic illustration of SnO₂/perovskite interfaces as passivated by adamantane derivative molecules.^[52] b) Grazing-incidence angle-dependent lattice spacings of perovskite films on SnO₂ ETLs with different molecular interfacial treatments.^[52] c) Theoretical models of SnO₂ and perovskite surfaces with different adamantane molecular passivators.^[52] d) Stability tests of control and target devices with molecular treatments under 60 °C thermal stress (top), continuous one-sun illumination (middle), and 15%–20% RH conditions (bottom).^[52] a–d) Reproduced with permission.^[52] Copyright 2022, Wiley-VCH.

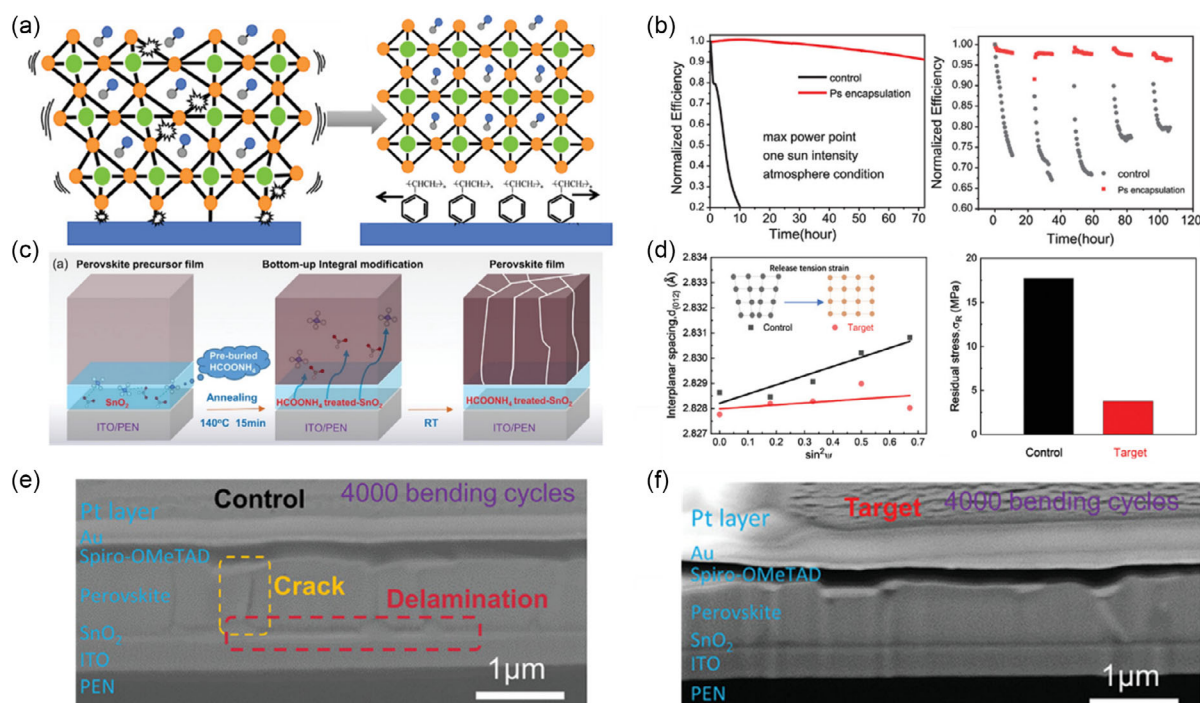


Figure 14. Residual stress release in perovskite layers via interfacial modifications. a) Schematic depiction of stress release of SnO₂/perovskite interface by PS layer.^[53] b) Operational stability under continuous one-sun illumination (left) and illumination–dark cycle stability (right) of PSC devices without and with PS buffer layer.^[53] a,b) Reproduced with permission.^[53] Copyright 2019, Wiley-VCH. c) Schematic illustration of preburied additive for cross-layer treatment of SnO₂/perovskite interface.^[44] d) d -spacing- $\sin^2\psi$ method for calculating the residual stress of perovskite films with and without NH₄COOH preburied additive.^[44] e,f) Cross-section SEM images of PSC devices after 4000 bending cycles with (e) and without (f) preburied NH₄COOH in SnO₂ ETLs.^[44] c–f) Reproduced with permission.^[44] Copyright 2022, Wiley-VCH.

interstitials (I_1^- and I_1^+) at the perovskite/charge transport layer interfaces; where electric-bias induced degradation also originated from the interaction between I_1^- and hole carriers transferred from ETL.^[54] Such device degradations as dictated by halide-defect formation and evolution behaviors thus signify discrepant passivation effects by different chemical treatments of SnO₂ ETLs.

3.3. Surface Composite-Structure Designs

From the energy level and electronic property perspectives, ETLs need to have high electron mobility, fine energy-level alignment, and good surface coverage of TCO substrates. Also, an optimized interfacial energy-level structure is exceptionally important to good charge extraction and transport, a basic requirement for reduced interfacial charge accumulation for good device stability.^[55,56] To meet these material characteristics, a meticulously composited ETL structure is demanded, such as double ETLs and planar/mesoporous composited structures, where Table 3 explicates a comprehensive summary of device performance and stability based on composite-structured ETL designs from recent works.

3.3.1. Suppressing Interfacial Charge Accumulation by Double Electron Transport Layers

Interfacial charge accumulation is detrimental to the stabilities of PSCs by accelerating ion migrations, thus triggering lattice

decomposition of perovskite materials.^[57] As a typical example, it was previously shown that the energy levels of SnO₂ ETLs can be effectively tuned by composing low-amount and high-amount NH₄Cl-doped composite SnO₂ ETLs (Figure 15a),^[58] in which the charge potential difference between composite SnO₂ ETLs and perovskite layers can be properly enlarged to promote light-induced charge extraction from the latter, thus facilitating the subsequent carrier transport to TCO substrate and avoiding charge accumulation (Figure 15b).^[58] A deeper mechanistic picture of the principles was further built, which needs to be followed for designing double ETLs, where composite order of TiO₂ and SnO₂ need to be scrutinized in terms of their free energy differences (ΔG) with perovskites and the resultant electron mobility within the ETLs (Figure 15c,d).^[59] Moreover, composite-structure designs featured with SnO₂-based dual ETLs in p–i–n structured PSCs have also been reported, where C₆₀/SnO₂ NCs and PCBM/SnO₂ NCs double ETLs were employed on top of perovskite layers to enhance electron extraction. These composite structures, as compared to pristine C₆₀ and PCBM ETLs, showed much more cascaded energy alignments with perovskites, thus resulting in mitigated hysteresis, overall performance, and long-term stability of PSCs.^[18,60] Based on these designing principles, researchers have constructed double ETLs with largely enhanced operational stabilities of the corresponding PSCs under different environmental stresses, whose performance and stability profiles are summarized in Table 3.

Table 3. Various approaches to enhance the stability of perovskite solar cells with double electron layers.

Double ETLs	Device architecture	Stability	Retained PCE	Ref.
TiO ₂ /SnO ₂	TCO/TiO ₂ /SnO ₂ /PVSK/HTL/Au	Unencapsulated, air, 80 °C, RH = 30%–35%, 200 h	95%	[39]
SnO ₂ /TiO ₂	ITO/SnO ₂ /TiO ₂ /PVSK/Spiro-OMeTAD/Au	Unencapsulated, N ₂ , no degradation after 49 days	\	[56b]
TiO ₂ /SnO ₂	FTO/TiO ₂ /SnO ₂ /PVSK/Spiro-OMeTAD/Au	Unencapsulated, N ₂ , RH = 0%, RT, AM1.5G, MPPT, ^{a)} 1000 h	97%	[79]
SnO ₂ +NH ₄ Cl/SnO ₂ +NH ₄ Cl	ITO/B-SnO ₂ /Perovskite/PEAI/Spiro-OMeTAD/Au	Unencapsulated, argon, RT, 90 days; Unencapsulated, AM1.5G, RT, 100 h	97.1% 86.5%	[58]
In ₂ O ₃ /SnO ₂	ITO/In ₂ O ₃ /SnO ₂ /PVSK/Spiro-OMeTAD/Au	Unencapsulated, N ₂ , 25 °C, 80 days; Unencapsulated, 1 sun, 180 h; Unencapsulated, RH = 75%, 120 h	97.5% 91% 80%	[55]
SnO ₂ /MgO	ITO/SnO ₂ /MgOPVSK/Spiro-OMeTAD/Au	Unencapsulated, RH < 30%, STC, ^{b)} dark, 107 days; AM1.5G, 100 mW cm ⁻² , MPPT, 107 days	68% 67.4%	[83]
SnO ₂ /DPC ₆₀ ^{c)}	ITO/SnO ₂ /DPC ₆₀ PVSK/HTL/Au	Unencapsulated, N ₂ , 1 sun, 55 ± 5 °C, MPPT, 200 h; Unencapsulated, RH = 35 ± 5%, 55 ± 5 °C, 30 days	82% 93%	[84]

^{a)}MPPT: maximum power point tracking; ^{b)}STC: standard test conditions (i.e., irradiance of 100 mW cm⁻², AM1.5G spectrum, at 25 °C); ^{c)}DPC₆₀: 2,5-diphenyl C₆₀ fulleropyrrolidine.

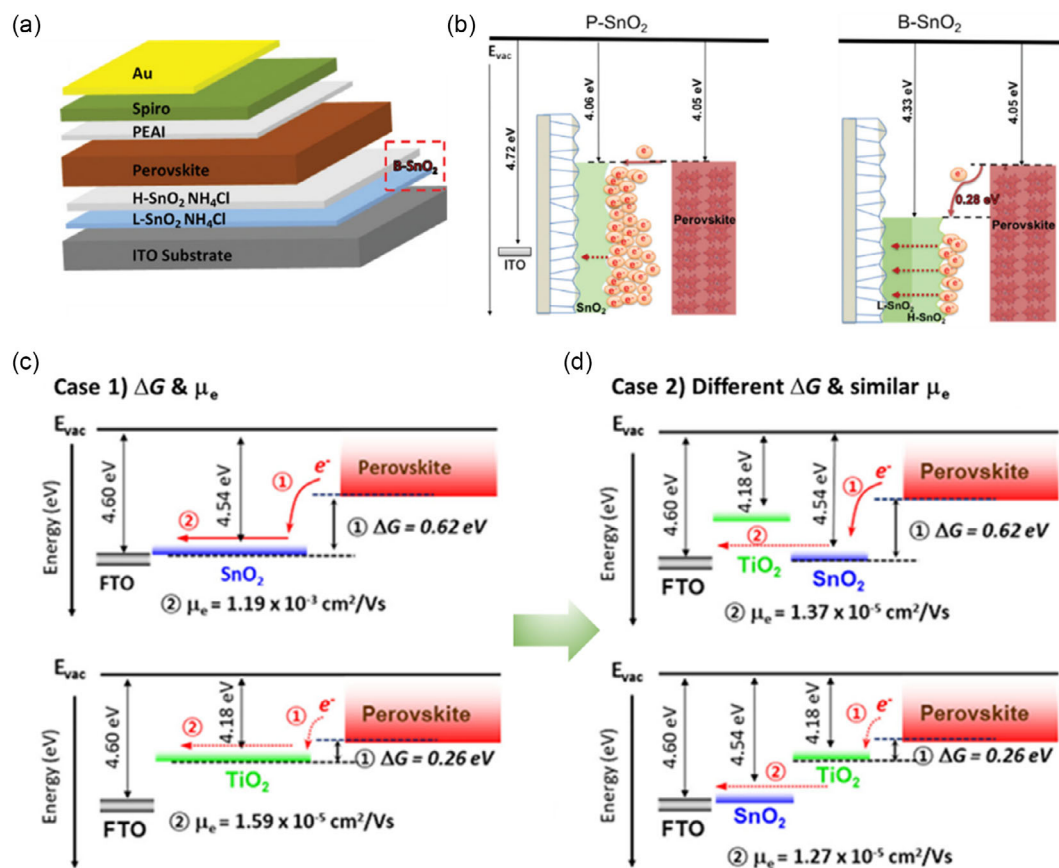


Figure 15. Double ETLs in PSCs for regulating energy-level alignments. a) Device structure of PSCs employing H-SnO₂ and L-SnO₂ double ETLs with NH₄Cl additive.^[58] b) Band alignment schematics of perovskite layers on single (left) and double (right) SnO₂ ETLs.^[58] a,b) Reproduced with permission.^[58] Copyright 2020, Wiley-VCH. c,d) Schematic diagrams of interfacial ΔG and μ_e with SnO₂ (top) and TiO₂ (bottom) being the single ETLs (c), and the arrangements of TiO₂/SnO₂ (top) and SnO₂/TiO₂ (bottom) being the double ETLs (d).^[59] c,d) Reproduced with permission.^[59] Copyright 2017, American Chemical Society.

3.3.2. Enhancing Mechanical Stability by Interpenetrative Electron Transport Layers

In addition to the interfacial charge accumulation, device stability is also dependent on the detailed surface morphological properties of ETL composites. Different from the mesoporous ETL structures, where the porosity of ETL materials such as TiO_2 is realized through thermal sintering the solution-deposited nanoparticle precursors,^[61] interpenetrative SnO_2 ETLs can also be achieved by the chemical reaction between the implanted precursor dopants therein and perovskite layers on the top. It was previously found that porous and interpenetrating SnO_2 ETL as generated from the evaporation of preburied formamidinium iodide (FAI) (Figure 16a) could lead to a more cascaded energy-level structure between SnO_2 and perovskites (Figure 16b).^[62] Also, the effects of the interpenetrating SnO_2 /perovskite interface can profoundly enhance physical adhesion of perovskite film on the SnO_2 ETL substrate, as manifested in the phenomenally enhanced mechanical strength that is free of interfacial delamination after bending stress (Figure 16d), in comparison with the perovskite film without the SnO_2 porosity treatment (Figure 16c).^[62] In the end, PSCs based on interpenetrating SnO_2 /perovskite interfacial design exhibited greater operational stability under

continuous one-sun illumination as imparted from maximum power point (MPP) tracking (Figure 16e) and mechanical durability of flexible PSCs with bending stress conditions (Figure 16f).^[62]

4. Summary and Outlook

This review analyzes the interconnection between SnO_2 ETLs and device stability as the focal point, with topics ranging from material properties and film formation of SnO_2 ETLs to the passivation and modification of interfacial defects. Summarizing the aforementioned works, degradations to the PV performance of PSCs related to the SnO_2 interface can be deduced into three categories: 1) surface defects of SnO_2 ETLs that facilitate the oxygen diffusion in perovskite layers that weaken the thermal/chemical stabilities of perovskite materials; 2) charge carrier accumulation and the related ion migration due to interfacial energy level misalignment, causing device instability under illumination and electrically biased conditions; and 3) interfacial stress induced by the lattice mismatch between perovskite and SnO_2 ETLs, causing weakened mechanical durability and performance degradation that are most significant in flexible PSCs. Accordingly, three manipulation strategies imposed on SnO_2 surface to tailor

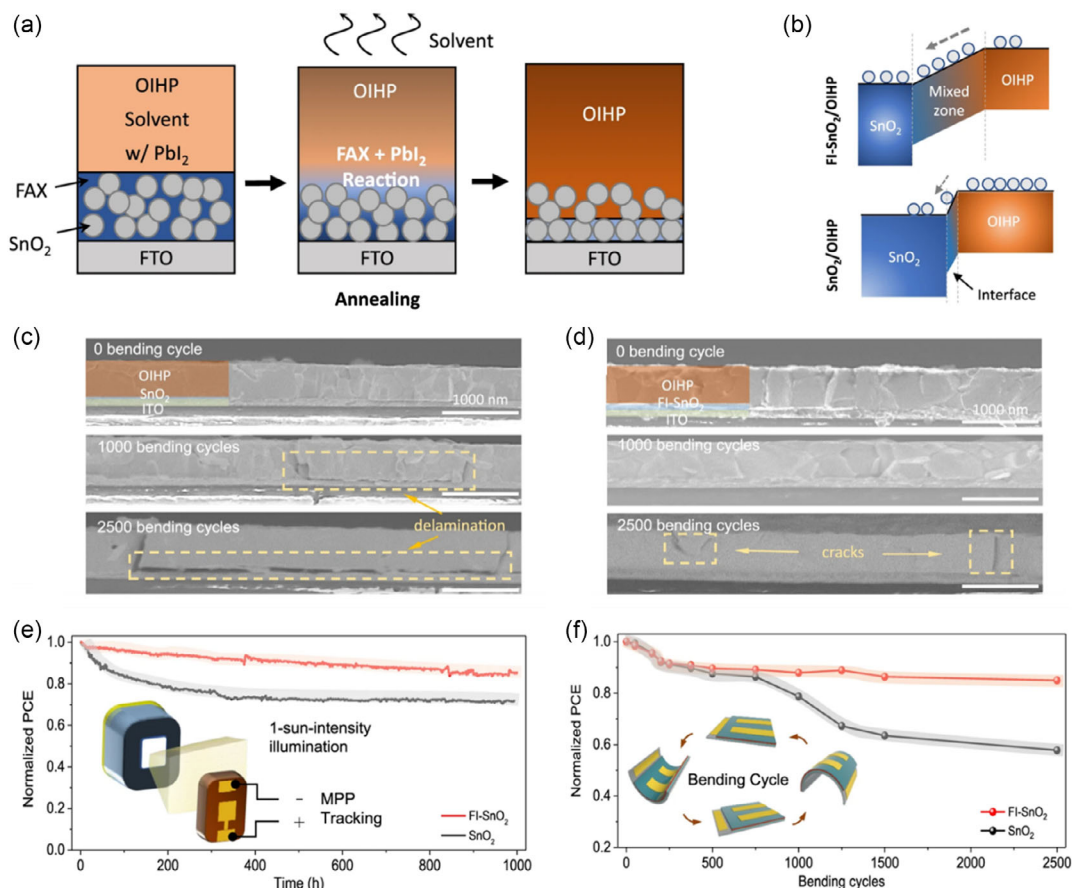


Figure 16. FAI-modified SnO_2 ETLs for interpenetrating interfaces in stable PSCs. a) Schematic illustrations of the preparation method of interpenetrative SnO_2 ETL and b) energy-level cascading between perovskite and pristine/interpenetrative SnO_2 ETLs.^[62] c) Cross-section SEM images of perovskite films deposited on pristine and d) interpenetrative SnO_2 ETLs before and after mechanical bending.^[62] e) Stability tests of rigid PSCs under continuous one-sun illumination and f) flexible PSCs with mechanical bending.^[62] a–f) Reproduced with permission.^[62] Copyright 2021, Springer Nature.

its physical and electronic compatibility in PSCs—surface morphological control, defect passivation, and composite-structure designs, have been utilized to improve the PSCs' PV performance and operational stability. Several substantiated conclusions are deduced as: 1) Surface morphological profiles of SnO₂ ETLs directly affect the film growth and crystallization quality of perovskite layers atop. 2) Hydroxyl groups and the existence of dangling bonds on the SnO₂ surface lead to reduced formation energy of oxygen vacancies that will accelerate deprotonation process of perovskite lattice under illumination and elevated temperature conditions, thus affecting stabilities under light and thermal stresses. 3) Composite-structure designs are conducive to reduced energy band offsets between ETLs and perovskites, thus inhibiting interfacial carrier accumulation and *J*–*V* hysteresis of PSCs.

In summary, surface modifications of SnO₂ ETLs have obtained prominent effects to the stability enhancement of PSCs against different environmental stresses, based on which we propose future research directions that were not fully accounted for in prior works, as detailed below.

4.1. Multifunctional Molecular Passivation

The defective buried interfaces of SnO₂/perovskite are complex physical and chemical systems, which not only involve surface defects such as hydroxyls and dangling bonds but also the causal lattice mismatch, interfacial delamination, and etc. Synergistic solution to all these problems demands customized passivation reagents (e.g., molecules with multiple functional groups, field-effect dipole molecules, polymers with special structural designs) with multiple functionality to simultaneously suppress surface defects of SnO₂ ETLs while gaining integrity of interfacial mechanics, so as to improve stability and PV performance at the same time.

4.2. SnO₂/Perovskite Integral Modifications

Even though SnO₂ has been optimized with tailored modifications that give rise to stable performance of PSCs, it is after all inorganic in chemical composition and has large bulk modulus. It thus constitutes phenomenal lattice mismatch and large thermal expansivity discrepancy with organic-contained perovskite films on top, thereby forming unavoidable interfacial residual stress upon film annealing. Therefore, constructing tailored interlayer designs is necessary to the strain relaxation at the buried interface, which is especially meaningful to the settings of flexible PSCs due to the massive thermally induced substrate deformation. Among the many manipulative routes, preburying volatile additives in SnO₂ ETL can lead to effective regulation of electron mobility, interfacial stress, and defect density of perovskite film as a whole, thus forming gradient distribution of additive ingredients across the SnO₂/perovskite interface.

4.3. Surface Composite-Structure Designs

In terms of double-ETL designs, while the bottom layer that interfaced with TCO substrates remain as planar structure, the top layer that contacts with perovskite can be selectively modified into porous or mesoporous morphology, which can accordingly

enlarge the contact area with perovskite for enhanced interfacial adhesion while fulfilling the cascaded energy level alignments for efficient carrier extraction/transport.

Acknowledgements

J.G. and Y.C. contributed equally to this work. This work was supported by the National Natural Science Foundation of China (62274026, 62004027, 52202216), the Central Government Guided Local Science and Technology Development Project of Sichuan Province (2021ZYD0048), and Sichuan Science and Technology Program (2023NSFSC0962).

Conflict of Interest

The authors declare no conflict of interest.

Keywords

defect passivation, operational stabilities, perovskite solar cells, SnO₂ electron transport layers, surface modifications

Received: December 9, 2022

Revised: February 20, 2023

Published online: April 12, 2023

- [1] H. Min, D. Y. Lee, J. Kim, G. Kim, K. S. Lee, J. Kim, M. J. Paik, Y. K. Kim, K. S. Kim, M. G. Kim, T. J. Shin, S. I. Seok, *Nature* **2021**, 598, 444.
- [2] D. Gao, B. Li, Z. Li, X. Wu, S. Zhang, D. Zhao, X. Jiang, C. Zhang, Y. Wang, Z. Li, N. Li, S. Xiao, W. C. H. Choy, A. K. Jen, S. Yang, Z. Zhu, *Adv Mater* **2022**, 35, 2206387.
- [3] N. Li, S. Tao, Y. Chen, X. Niu, C. K. Onwudinanti, C. Hu, Z. Qiu, Z. Xu, G. Zheng, L. Wang, Y. Zhang, L. Li, H. Liu, Y. Lun, J. Hong, X. Wang, Y. Liu, H. Xie, Y. Gao, Y. Bai, S. Yang, G. Brocks, Q. Chen, H. Zhou, *Nat. Energy* **2019**, 4, 408.
- [4] a) Z. Liu, L. Qiu, L. K. Ono, S. He, Z. Hu, M. Jiang, G. Tong, Z. Wu, Y. Jiang, D.-Y. Son, Y. Dang, S. Kazaoui, Y. Qi, *Nat. Energy* **2020**, 5, 596; b) Q. Jiang, D. Rebolgar, J. Gong, E. L. Piacentino, C. Zheng, T. Xu, *Angew. Chem., Int. Ed.* **2015**, 54, 7617; c) Y. Wang, T. Wu, J. Barbaud, W. Kong, D. Cui, H. Chen, X. Yang, L. Han, *Science* **2019**, 365, 687; d) B. Liu, H. Bi, D. He, L. Bai, W. Wang, H. Yuan, Q. Song, P. Su, Z. Zang, T. Zhou, J. Chen, *ACS Energy Lett.* **2021**, 6, 2526; e) J. A. Christians, P. Schulz, J. S. Tinkham, T. H. Schloemer, S. P. Harvey, B. J. Tremolet de Villers, A. Sellinger, J. J. Berry, J. M. Luther, *Nat. Energy* **2018**, 3, 68; f) B. Liu, Y. Wang, Y. Wu, Y. Zhang, J. Lyu, Z. Liu, S. Bian, X. Bai, L. Xu, D. Zhou, B. Dong, H. Song, *Adv. Energy Mater.* **2022**, 13, 202203352; g) Y. Liu, F. Li, J. Gong, M. Liu, *ACS Energy Lett.* **2022**, 7, 3227.
- [5] a) Q. Jiang, Y. Zhao, X. Zhang, X. Yang, Y. Chen, Z. Chu, Q. Ye, X. Li, Z. Yin, J. You, *Nat. Photonics* **2019**, 13, 460; b) Y. Zhao, I. Yavuz, M. Wang, M. H. Weber, M. Xu, J. H. Lee, S. Tan, T. Huang, D. Meng, R. Wang, J. Xue, S. J. Lee, S. H. Bae, A. Zhang, S. G. Choi, Y. Yin, J. Liu, T. H. Han, Y. Shi, H. Ma, W. Yang, Q. Xing, Y. Zhou, P. Shi, S. Wang, E. Zhang, J. Bian, X. Pan, N. G. Park, J. W. Lee, Y. Yang, *Nat. Mater.* **2022**, 21, 1396; c) P. Calado, A. M. Telford, D. Bryant, X. Li, J. Nelson, B. C. O'Regan, P. R. Barnes, *Nat. Commun.* **2016**, 7, 13831.
- [6] a) J. Xia, Y. Zhang, C. Xiao, K. G. Brooks, M. Chen, J. Luo, H. Yang, N. I. D. Klipfel, J. Zou, Y. Shi, X. Yao, J. Chen, J. M. Luther, H. Lin,

- A. M. Asiri, C. Jia, M. K. Nazeeruddin, *Joule* **2022**, 6, 1689; b) T. Zhang, F. Wang, H.-B. Kim, I.-W. Choi, C. Wang, E. Cho, R. Konefal, Y. Puttisong, K. Terado, L. Kobera, M. Chen, M. Yang, S. Bai, B. Yang, J. Suo, S.-C. Yang, X. Liu, F. Fu, H. Yoshida, W. M. Chen, J. Brus, V. Coropceanu, A. Hagfeldt, J.-L. Brédas, M. Fahlman, D. S. Kim, Z. Hu, F. Gao, *Science* **2022**, 377, 495.
- [7] a) B. Roose, C. M. Johansen, K. Dupraz, T. Jaouen, P. Aebi, U. Steiner, A. Abate, *J. Mater. Chem. A* **2018**, 6, 1850; b) W. Hui, Y. Yang, Q. Xu, H. Gu, S. Feng, Z. Su, M. Zhang, J. Wang, X. Li, J. Fang, F. Xia, Y. Xia, Y. Chen, X. Gao, W. Huang, *Adv. Mater.* **2020**, 32, 1906374; c) Z. Liu, K. Deng, J. Hu, L. Li, *Angew. Chem., Int. Ed.* **2019**, 58, 11497.
- [8] a) J. Liu, S. Li, S. Liu, Y. Chu, T. Ye, C. Qiu, Z. Qiu, X. Wang, Y. Wang, Y. Su, Y. Hu, Y. Rong, A. Mei, H. Han, *Angew. Chem., Int. Ed.* **2022**, 61, e202202012; b) E. Jiang, Y. Ai, J. Yan, N. Li, L. Lin, Z. Wang, C. Shou, B. Yan, Y. Zeng, J. Sheng, J. Ye, *ACS Appl. Mater. Interfaces* **2019**, 11, 36727; c) E. Jiang, J. Yan, Y. Ai, N. Li, B. Yan, Y. Zeng, J. Sheng, J. Ye, *Mater. Today Energy* **2019**, 12, 389; d) E. H. Jung, B. Chen, K. Bertens, M. Vafaie, S. Teale, A. Proppe, Y. Hou, T. Zhu, C. Zheng, E. H. Sargent, *ACS Energy Lett.* **2020**, 5, 2796.
- [9] J. Song, H. Liu, W. Pu, Y. Lu, Z. Si, Z. Zhang, Y. Ge, N. Li, H. Zhou, W. Xiao, L. Wang, M. Sui, *Energy Environ. Sci.* **2022**, 15, 4836.
- [10] a) C. Altinkaya, E. Aydin, E. Ugur, F. H. Isikgor, A. S. Subbiah, M. De Bastiani, J. Liu, A. Babayigit, T. G. Allen, F. Laquai, A. Yildiz, S. De Wolf, *Adv. Mater.* **2021**, 33, 2005504; b) S. Y. Park, K. Zhu, *Adv. Mater.* **2022**, 34, 2110438; c) P. Wu, S. Wang, X. Li, F. Zhang, *J. Mater. Chem. A* **2021**, 9, 19554.
- [11] V. B. Kamble, A. M. Umarji, *AIP Adv.* **2013**, 3, 082120.
- [12] X. Chen, L. Liu, F. Huang, *Chem. Soc. Rev.* **2015**, 44, 1861.
- [13] J. Tauc, R. Grigorovici, A. Vancu, *Phys. Status Solidi B* **1966**, 15, 627.
- [14] a) W. Ke, G. Fang, Q. Liu, L. Xiong, P. Qin, H. Tao, J. Wang, H. Lei, B. Li, J. Wan, G. Yang, Y. Yan, *J. Am. Chem. Soc.* **2015**, 137, 6730; b) E. H. Anaraki, A. Kermanpur, L. Steier, K. Domanski, T. Matsui, W. Tress, M. Saliba, A. Abate, M. Grätzel, A. Hagfeldt, J.-P. Correa-Baena, *Energy Environ. Sci.* **2016**, 9, 3128; c) Q. Jiang, Z. Chu, P. Wang, X. Yang, H. Liu, Y. Wang, Z. Yin, J. Wu, X. Zhang, J. You, *Adv. Mater.* **2017**, 29, 1703852; d) D. Yang, R. Yang, K. Wang, C. Wu, X. Zhu, J. Feng, X. Ren, G. Fang, S. Priya, S. F. Liu, *Nat. Commun.* **2018**, 9, 3239; e) Y.-W. Jang, S. Lee, K. M. Yeom, K. Jeong, K. Choi, M. Choi, J. H. Noh, *Nat. Energy* **2021**, 6, 63; f) NREL solar cell efficiency chart, <https://www.nrel.gov/pv/interactive-cell-efficiency.html>
- [15] D. Wang, S.-C. Chen, Q. Zheng, *J. Mater. Chem. C* **2019**, 7, 12204.
- [16] L. Xiong, M. Qin, G. Yang, Y. Guo, H. Lei, Q. Liu, W. Ke, H. Tao, P. Qin, S. Li, H. Yu, G. Fang, *J. Mater. Chem. A* **2016**, 4, 8374.
- [17] R. Yuan, B. Cai, Y. Lv, X. Gao, J. Gu, Z. Fan, X. Liu, C. Yang, M. Liu, W.-H. Zhang, *Energy Environ. Sci.* **2021**, 14, 5074.
- [18] Y. Wang, C. Duan, J. Li, W. Han, M. Zhao, L. Yao, Y. Wang, C. Yan, T. Jiu, *ACS Appl. Mater. Interfaces* **2018**, 10, 20128.
- [19] J. J. Yoo, G. Seo, M. R. Chua, T. G. Park, Y. Lu, F. Rotermund, Y. K. Kim, C. S. Moon, N. J. Jeon, J. P. Correa-Baena, V. Bulovic, S. S. Shin, M. G. Bawendi, J. Seo, *Nature* **2021**, 590, 587.
- [20] a) Z. Song, W. Bi, X. Zhuang, Y. Wu, B. Zhang, X. Chen, C. Chen, Q. Dai, H. Song, *Sol. RRL* **2020**, 4, 1900266; b) K. Choi, J. Lee, H. I. Kim, C. W. Park, G.-W. Kim, H. Choi, S. Park, S. A. Park, T. Park, *Energy Environ. Sci.* **2018**, 11, 3238; c) J. P. C. Baena, L. Steier, W. Tress, M. Saliba, S. Neutzner, T. Matsui, F. Giordano, T. J. Jacobsson, A. R. S. Kandada, S. M. Zakeeruddin, *Energy Environ. Sci.* **2015**, 8, 2928; d) Q. Jiang, L. Zhang, H. Wang, X. Zhang, J. Meng, H. Liu, Z. Yin, J. Wu, X. Zhang, J. You, *Nat. Energy* **2016**, 2, 16177; e) M. Kam, Q. Zhang, D. Zhang, Z. Fan, *Sci. Rep.* **2019**, 9, 6963.
- [21] L. Kavan, L. Steier, M. Grätzel, *J. Phys. Chem. C* **2016**, 121, 342.
- [22] R. M. Pasquarelli, D. S. Ginley, R. O'Hayre, *Chem. Soc. Rev.* **2011**, 40, 5406.
- [23] a) C. Xu, Z. Liu, Q. Sun, E.-C. Lee, *Sol. Energy* **2021**, 214, 280; b) G. Yang, C. Chen, F. Yao, Z. Chen, Q. Zhang, X. Zheng, J. Ma, H. Lei, P. Qin, L. Xiong, W. Ke, G. Li, Y. Yan, G. Fang, *Adv. Mater.* **2018**, 30, 1706023.
- [24] a) D. P. McMeekin, P. Holzhey, S. O. Furer, S. P. Harvey, L. T. Schelhas, J. M. Ball, S. Mahesh, S. Seo, N. Hawkins, J. Lu, M. B. Johnston, J. J. Berry, U. Bach, H. J. Snaith, *Nat. Mater.* **2022**, 22, 73; b) C. H. Chen, Z. H. Su, Y. H. Lou, Y. J. Yu, K. L. Wang, G. L. Liu, Y. R. Shi, J. Chen, J. J. Cao, L. Zhang, X. Y. Gao, Z. K. Wang, *Adv. Mater.* **2022**, 34, 2200320.
- [25] T. Bu, L. K. Ono, J. Li, J. Su, G. Tong, W. Zhang, Y. Liu, J. Zhang, J. Chang, S. Kazaoui, F. Huang, Y.-B. Cheng, Y. Qi, *Nat. Energy* **2022**, 7, 528.
- [26] L. Qiu, Z. Liu, L. K. Ono, Y. Jiang, D. Y. Son, Z. Hawash, S. He, Y. Qi, *Adv. Funct. Mater.* **2018**, 29, 1806779.
- [27] L. Xiong, J. Li, F. Ye, H. Wang, Y. Guo, X. Ming, Q. Chen, S. Zhang, R. Xie, Z. Chen, Y. Lv, G. Hu, Y. He, G. Fang, *Adv. Funct. Mater.* **2021**, 31, 2103949.
- [28] Y. Rong, Y. Hu, A. Mei, H. Tan, M. I. Saidaminov, S. I. Seok, M. D. McGehee, E. H. Sargent, H. Han, *Science* **2018**, 361, eaat8235.
- [29] a) B. Roose, J.-P. C. Baena, K. C. Gödel, M. Graetzel, A. Hagfeldt, U. Steiner, A. Abate, *Nano Energy* **2016**, 30, 517; b) S. Lin, B. Yang, X. Qiu, J. Yan, J. Shi, Y. Yuan, W. Tan, X. Liu, H. Huang, Y. Gao, C. Zhou, *Org. Electron.* **2018**, 53, 235.
- [30] P. F. Méndez, S. K. M. Muhammed, E. M. Barea, S. Masi, I. Mora-Seró, *Sol. RRL* **2019**, 3, 1900191.
- [31] Q. Dong, J. Li, Y. Shi, M. Chen, L. K. Ono, K. Zhou, C. Zhang, Y. Qi, Y. Zhou, N. P. Padture, *Adv. Mater.* **2019**, 9, 1900834.
- [32] S. You, H. Zeng, Z. Ku, X. Wang, Z. Wang, Y. Rong, Y. Zhao, X. Zheng, L. Luo, L. Li, S. Zhang, M. Li, X. Gao, X. Li, *Adv. Mater.* **2020**, 32, 2003990.
- [33] H. Dong, J. Wang, X. Li, W. Liu, T. Xia, D. Yao, L. Zhang, C. Zuo, L. Ding, F. Long, *ACS Appl. Mater. Interfaces* **2022**, 14, 34143.
- [34] a) X. Zhang, Y. Rui, Y. Wang, J. Xu, H. Wang, Q. Zhang, P. Müller-Buschbaum, *J. Power Sources* **2018**, 402, 460; b) C. Gao, S. Yuan, B. Cao, J. Yu, *Chem. Eng. J.* **2017**, 325, 378; c) S. S. Mali, J. V. Patil, H. Kim, C. K. Hong, *Nanoscale* **2018**, 10, 8275; d) X. Wu, Y. Zheng, J. Liang, Z. Zhang, C. Tian, Z. Zhang, Y. Hu, A. Sun, C. Wang, J. Wang, Y. Huang, Z. Zhang, K. M. Reddy, C. C. Chen, *Mater. Horiz.* **2023**, 10, 122.
- [35] X. Zhang, Y. Rui, J. Yang, L. Wang, Y. Wang, J. Xu, *Appl. Surf. Sci.* **2019**, 463, 679.
- [36] H. Huang, X. Liu, M. Duan, J. Ji, H. Jiang, B. Liu, S. Sajid, P. Cui, D. Wei, Y. Li, M. Li, *ACS Appl. Energy Mater.* **2020**, 3, 5039.
- [37] R. Keshtmand, M. R. Zamani-Meymian, F. Mohamadkhani, N. Taghavinia, *Sol. Energy* **2021**, 228, 253.
- [38] H. Bi, B. Liu, D. He, L. Bai, W. Wang, Z. Zang, J. Chen, *Chem. Eng. J.* **2021**, 418, 129375.
- [39] S. S. Mali, J. V. Patil, H. Arandian, C. K. Hong, *J. Mater. Chem. A* **2019**, 7, 17516.
- [40] H. Feng, S. Liu, G. Tang, L. Zhang, W. Xie, *J. Mater. Chem. C* **2021**, 9, 13748.
- [41] K. Jung, D. H. Kim, J. Kim, S. Ko, J. W. Choi, K. C. Kim, S.-G. Lee, M.-J. Lee, *J. Mater. Sci. Technol.* **2020**, 59, 195.
- [42] Z. Xiong, X. Chen, B. Zhang, G. O. Odunmbaku, Z. Ou, B. Guo, K. Yang, Z. Kan, S. Lu, S. Chen, N. A. N. Ouedraogo, Y. Cho, C. Yang, J. Chen, K. Sun, *Adv. Mater.* **2022**, 34, 2106118.
- [43] Y. Dong, W. Shen, W. Dong, C. Bai, J. Zhao, Y. Zhou, F. Huang, Y. B. Cheng, J. Zhong, *Adv. Mater.* **2022**, 12, 2200417.
- [44] Z. Zheng, F. Li, J. Gong, Y. Ma, J. Gu, X. Liu, S. Chen, M. Liu, *Adv. Mater.* **2022**, 34, 2109879.

- [45] H. Liu, Z. Zhang, Z. Su, W. Zuo, Y. Tang, F. Yang, X. Zhang, C. Qin, J. Yang, Z. Li, M. Li, *Adv. Sci.* **2022**, 9, 2105739.
- [46] L. Yang, J. Feng, Z. Liu, Y. Duan, S. Zhan, S. Yang, K. He, Y. Li, Y. Zhou, N. Yuan, J. Ding, S. F. Liu, *Adv. Mater.* **2022**, 34, 2201681.
- [47] a) A. Ulman, *Chem. Rev.* **1996**, 96, 1533; b) L. Zuo, Z. Gu, T. Ye, W. Fu, G. Wu, H. Li, H. Chen, *J. Am. Chem. Soc.* **2015**, 137, 2674; c) M. Hou, H. Zhang, Z. Wang, Y. Xia, Y. Chen, W. Huang, *ACS Appl. Mater. Interfaces* **2018**, 10, 30607; d) S. Y. Kim, S. J. Cho, S. E. Byeon, X. He, H. J. Yoon, *Adv. Energy Mater.* **2020**, 10, 2002606.
- [48] F. Ali, C. Roldán-Carmona, M. Sohail, M. K. Nazeeruddin, *Adv. Energy Mater.* **2020**, 10, 2002989.
- [49] Z. Dai, S. K. Yadavalli, M. Chen, A. Abbaspourtamijani, Y. Qi, N. P. Padture, *Science* **2021**, 372, 618.
- [50] Z. Dai, S. Li, X. Liu, M. Chen, C. E. Athanasiou, B. W. Sheldon, H. Gao, P. Guo, N. P. Padture, *Adv. Mater.* **2022**, 34, 2205301.
- [51] a) H. Wang, C. Zhu, L. Liu, S. Ma, P. Liu, J. Wu, C. Shi, Q. Du, Y. Hao, S. Xiang, H. Chen, P. Chen, Y. Bai, H. Zhou, Y. Li, Q. Chen, *Adv. Mater.* **2019**, 31, 1904408; b) C. Zhu, X. Niu, Y. Fu, N. Li, C. Hu, Y. Chen, X. He, G. Na, P. Liu, H. Zai, Y. Ge, Y. Lu, X. Ke, Y. Bai, S. Yang, P. Chen, Y. Li, M. Sui, L. Zhang, H. Zhou, Q. Chen, *Nat. Commun.* **2019**, 10, 815; c) D. J. Xue, Y. Hou, S. C. Liu, M. Wei, B. Chen, Z. Huang, Z. Li, B. Sun, A. H. Proppe, Y. Dong, M. I. Saidaminov, S. O. Kelley, J. S. Hu, E. H. Sargent, *Nat. Commun.* **2020**, 11, 1514; d) J. Zhao, Y. Deng, H. Wei, X. Zheng, Z. Yu, Y. Shao, J. E. Shield, J. Huang, *Sci. Adv.* **2017**, 3, eaao5616; e) Q. Zhou, J. Duan, X. Yang, Y. Duan, Q. Tang, *Angew. Chem., Int. Ed.* **2020**, 59, 21997.
- [52] Q. Zhou, D. He, Q. Zhuang, B. Liu, R. Li, H. Li, Z. Zhang, H. Yang, P. Zhao, Y. He, Z. Zang, J. Chen, *Adv. Funct. Mater.* **2022**, 32, 2205507.
- [53] J. Wu, Y. Cui, B. Yu, K. Liu, Y. Li, H. Li, J. Shi, H. Wu, Y. Luo, D. Li, Q. Meng, *Adv. Funct. Mater.* **2019**, 29, 1905336.
- [54] Z. Ni, H. Jiao, C. Fei, H. Gu, S. Xu, Z. Yu, G. Yang, Y. Deng, Q. Jiang, Y. Liu, Y. Yan, J. Huang, *Nat. Energy* **2021**, 7, 65.
- [55] P. Wang, R. Li, B. Chen, F. Hou, J. Zhang, Y. Zhao, X. Zhang, *Adv. Mater.* **2020**, 32, 1905766.
- [56] a) Y. Hou, X. Chen, S. Yang, C. Li, H. Zhao, H. G. Yang, *Adv. Funct. Mater.* **2017**, 27, 1700878; b) M. Hu, L. Zhang, S. She, J. Wu, X. Zhou, X. Li, D. Wang, J. Miao, G. Mi, H. Chen, Y. Tian, B. Xu, C. Cheng, *Sol. RRL* **2019**, 4, 1900331; c) Q. Liu, M.-C. Qin, W.-J. Ke, X.-L. Zheng, Z. Chen, P.-L. Qin, L.-B. Xiong, H.-W. Lei, J.-W. Wan, J. Wen, G. Yang, J.-J. Ma, Z.-Y. Zhang, G.-J. Fang, *Adv. Funct. Mater.* **2016**, 26, 6069; d) M. M. Tavakoli, F. Giordano, S. M. Zakeeruddin, M. Gratzel, *Nano Lett.* **2018**, 18, 2428; e) Q. Liu, M.-C. Qin, W.-J. Ke, X.-L. Zheng, Z. Chen, P.-L. Qin, L.-B. Xiong, H.-W. Lei, J.-W. Wan, J. Wen, G. Yang, J.-J. Ma, Z.-Y. Zhang, G.-J. Fang, *Adv. Funct. Mater.* **2016**, 26, 6069; f) M. M. Tavakoli, F. Giordano, S. M. Zakeeruddin, M. Gratzel, *Nano Lett.* **2018**, 18, 2428; g) F. Li, Y. Xie, Y. Hu, M. Long, Y. Zhang, J. Xu, M. Qin, X. Lu, M. Liu, *ACS Energy Lett.* **2020**, 5, 1422; h) F. Li, Y. Xie, Y. Hu, M. Long, Y. Zhang, J. Xu, M. Qin, X. Lu, M. Liu, *ACS Energy Lett.* **2020**, 5, 1422; i) L. Mao, T. Yang, H. Zhang, J. Shi, Y. Hu, P. Zeng, F. Li, J. Gong, X. Fang, Y. Sun, X. Liu, J. Du, A. Han, L. Zhang, W. Liu, F. Meng, X. Cui, Z. Liu, M. Liu, *Adv. Mater.* **2022**, 34, 2206193.
- [57] S. Tan, T. Huang, I. Yavuz, R. Wang, T. W. Yoon, M. Xu, Q. Xing, K. Park, D. K. Lee, C. H. Chen, R. Zheng, T. Yoon, Y. Zhao, H. C. Wang, D. Meng, J. Xue, Y. J. Song, X. Pan, N. G. Park, J. W. Lee, Y. Yang, *Nature* **2022**, 605, 268.
- [58] J. Ye, Y. Li, A. A. Medjahed, S. Pouget, D. Aldakov, Y. Liu, P. Reiss, *Small* **2021**, 17, 2005671.
- [59] S. Song, G. Kang, L. Pyeon, C. Lim, G.-Y. Lee, T. Park, J. Choi, *ACS Energy Lett.* **2017**, 2, 2667.
- [60] J. Liu, Y. Guo, M. Zhu, Y. Li, X. Li, *J. Power Sources* **2020**, 476, 228648.
- [61] M. M. Lee, J. Teuscher, T. Miyasaka, T. N. Murakami, H. J. Snaith, *Science* **2012**, 338, 643.
- [62] Q. Dong, C. Zhu, M. Chen, C. Jiang, J. Guo, Y. Feng, Z. Dai, S. K. Yadavalli, M. Hu, X. Cao, Y. Li, Y. Huang, Z. Liu, Y. Shi, L. Wang, N. P. Padture, Y. Zhou, *Nat. Commun.* **2021**, 12, 973.
- [63] a) C. Wang, L. Guan, D. Zhao, Y. Yu, C. R. Grice, Z. Song, R. A. Awani, J. Chen, J. Wang, X. Zhao, Y. Yan, *ACS Energy Lett.* **2017**, 2, 2118; b) J. Feng, X. Zhu, Z. Yang, X. Zhang, J. Niu, Z. Wang, S. Zuo, S. Priya, S. F. Liu, D. Yang, *Adv. Mater.* **2018**, 30, 1801418; c) S. Wu, Z. Li, J. Zhang, X. Wu, X. Deng, Y. Liu, J. Zhou, C. Zhi, X. Yu, W. C. H. Choy, Z. Zhu, A. K. Jen, *Adv. Mater.* **2021**, 33, 2105539; d) D. Yang, R. Yang, X. Ren, X. Zhu, Z. Yang, C. Li, S. F. Liu, *Adv. Mater.* **2016**, 28, 5206; e) K. Huang, Y. Peng, Y. Gao, J. Shi, H. Li, X. Mo, H. Huang, Y. Gao, L. Ding, J. Yang, *Adv. Energy Mater.* **2019**, 9, 1901419; f) B. J. Kim, D. H. Kim, Y.-Y. Lee, H.-W. Shin, G. S. Han, J. S. Hong, K. Mahmood, T. K. Ahn, Y.-C. Joo, K. S. Hong, N.-G. Park, S. Lee, H. S. Jung, *Energy Environ. Sci.* **2015**, 8, 916; g) M. Li, J. Zhou, L. Tan, H. Li, Y. Liu, C. Jiang, Y. Ye, L. Ding, W. Tress, C. Yi, *Innovation* **2022**, 3, 100310; h) L. Yang, Q. Xiong, Y. Li, P. Gao, B. Xu, H. Lin, X. Li, T. Miyasaka, *Journal of Mater. Chem. A* **2021**, 9, 1574; i) M. Park, J.-Y. Kim, H. J. Son, C.-H. Lee, S. S. Jang, M. J. Ko, *Nano Energy* **2016**, 26, 208; j) P. Docampo, J. M. Ball, M. Darwich, G. E. Eperon, H. J. Snaith, *Nat. Commun.* **2013**, 4, 2761; k) S. S. Shin, W. S. Yang, J. H. Noh, J. H. Suk, N. J. Jeon, J. H. Park, J. S. Kim, W. M. Seong, S. I. Seok, *Nat. Commun.* **2015**, 6, 7410; l) C. Long, K. Huang, J. Chang, C. Zuo, Y. Gao, X. Luo, B. Liu, H. Xie, Z. Chen, J. He, H. Huang, Y. Gao, L. Ding, J. Yang, *Small* **2021**, 17, 2102368.
- [64] T. Bu, J. Li, F. Zheng, W. Chen, X. Wen, Z. Ku, Y. Peng, J. Zhong, Y. B. Cheng, F. Huang, *Nat. Commun.* **2018**, 9, 4609.
- [65] a) P. Schulz, J. O. Tiepelt, J. A. Christians, I. Levine, E. Edri, E. M. Sanehira, G. Hodes, D. Cahen, A. Kahn, *ACS Appl. Mater. Interfaces* **2016**, 8, 31491; b) A. Agresti, A. Pazniak, S. Pescetelli, A. Di Vito, D. Rossi, A. Pecchia, M. Auf der Maur, A. Liedl, R. Larciprete, D. V. Kuznetsov, D. Saranin, A. Di Carlo, *Nat. Mater.* **2019**, 18, 1228.
- [66] J. Kim, G. Kim, T. K. Kim, S. Kwon, H. Back, J. Lee, S. H. Lee, H. Kang, K. Lee, *J. Mater. Chem. A* **2014**, 2, 17291.
- [67] a) B. Roose, Q. Wang, A. Abate, *Adv. Energy Mater.* **2019**, 9, 1803140; b) S. Ye, W. Sun, Y. Li, W. Yan, H. Peng, Z. Bian, Z. Liu, C. Huang, *Nano Lett.* **2015**, 15, 3723.
- [68] a) W. Chen, F. Z. Liu, X. Y. Feng, A. B. Djurišić, W. K. Chan, Z. B. He, *Adv. Energy Mater.* **2017**, 7, 1700722; b) S. Wu, R. Chen, S. Zhang, B. H. Babu, Y. Yue, H. Zhu, Z. Yang, C. Chen, W. Chen, Y. Huang, S. Fang, T. Liu, L. Han, W. Chen, *Nat. Commun.* **2019**, 10, 1161.
- [69] a) X. Ye, H. Ling, R. Zhang, Z. Wen, S. Hu, T. Akasaka, J. Xia, X. Lu, J. Power Sources **2020**, 448, 227419; b) F. Zhao, Y. Guo, X. Wang, J. Tao, J. Jiang, Z. Hu, J. Chu, *Sol. Energy* **2019**, 191, 263.
- [70] a) X. Wang, L.-L. Deng, L.-Y. Wang, S.-M. Dai, Z. Xing, X.-X. Zhan, X.-Z. Lu, S.-Y. Xie, R.-B. Huang, L.-S. Zheng, *J. Mater. Chem. A* **2017**, 5, 1706; b) J. Yang, Q. Zhang, J. Xu, H. Liu, R. Qin, H. Zhai, S. Chen, M. Yuan, *Nanomaterials* **2019**, 9, 1666.
- [71] a) Q. Luo, H. Chen, Y. Lin, H. Du, Q. Hou, F. Hao, N. Wang, Z. Guo, J. Huang, *Adv. Funct. Mater.* **2017**, 27, 1702090; b) W. Zhu, Q. Zhang, C. Zhang, D. Chen, L. Zhou, Z. Lin, J. Chang, J. Zhang, Y. Hao, *Dalton Trans.* **2018**, 47, 6404; c) W. Hu, T. Liu, X. Yin, H. Liu, X. Zhao, S. Luo, Y. Guo, Z. Yao, J. Wang, N. Wang, *J. Mater. Chem. A* **2017**, 5, 1434; d) Y. Guo, T. Liu, N. Wang, Q. Luo, H. Lin, J. Li, Q. Jiang, L. Wu, Z. Guo, *Nano Energy* **2017**, 38, 193.
- [72] a) J. J. M. Vequizo, M. Yokoyama, M. Ichimura, A. Yamakata, *Appl. Phys. Express* **2016**, 9, 067101; b) J. J. Choi, X. Yang, Z. M. Norman, S. J. Billinge, J. S. Owen, *Nano Lett.* **2014**, 14, 127.
- [73] J. Song, E. Zheng, J. Bian, X.-F. Wang, W. Tian, Y. Sanehira, T. Miyasaka, *J. Mater. Chem. A* **2015**, 3, 10837.

- [74] W.-Q. Wu, D. Chen, Y.-B. Cheng, R. A. Caruso, *Sol. RRL* **2017**, *1*, 1700117.
- [75] X. Liu, Y. Zhang, L. Shi, Z. Liu, J. Huang, J. S. Yun, Y. Zeng, A. Pu, K. Sun, Z. Hameiri, J. A. Stride, J. Seidel, M. A. Green, X. Hao, *Adv. Mater.* **2018**, *8*, 1800138.
- [76] S. Akin, *ACS Appl. Mater. Interfaces* **2019**, *11*, 39998.
- [77] P. Hang, J. Xie, G. Li, Y. Wang, D. Fang, Y. Yao, D. Xie, C. Cui, K. Yan, J. Xu, D. Yang, X. Yu, *iScience* **2019**, *21*, 217.
- [78] X. Chen, W. Xu, Z. Shi, G. Pan, J. Zhu, J. Hu, X. Li, C. Shan, H. Song, *Nano Energy* **2021**, *80*, 105564.
- [79] M. Abuhelaiqa, N. Shibayama, X.-X. Gao, H. Kanda, M. K. Nazeeruddin, *ACS Appl. Energy Mater.* **2021**, *4*, 3424.
- [80] Z. Qin, Y. Chen, X. Wang, N. Wei, X. Liu, H. Chen, Y. Miao, Y. Zhao, *Adv. Mater.* **2022**, *34*, 2203143.
- [81] G. Mathiazhagan, A. Seeber, T. Gengenbach, S. Mastroianni, D. Vak, A. S. R. Chesman, M. Gao, D. Angmo, A. Hinsch, *Sol. RRL* **2020**, *4*, 2000262.
- [82] J. Chen, X. Zhao, S. G. Kim, N. G. Park, *Adv. Mater.* **2019**, *31*, 1902902.
- [83] J. Dagar, S. Castro-Hermosa, G. Lucarelli, F. Cacialli, T. M. Brown, *Nano Energy* **2018**, *49*, 290.
- [84] C. Tian, K. Lin, J. Lu, W. Feng, P. Song, L. Xie, Z. Wei, *Small Methods* **2019**, *4*, 1900476.



Jue Gong received his Ph.D. degree from Northern Illinois University, USA, in 2018. He joined University of Electronic Science and Technology of China in 2021 as an associate professor. His research focuses on flexible perovskite solar cells.



Yupeng Cui received his Bachelor's degree in 2020 from Shandong Technology and Business University. His research focuses on high-performance and stable perovskite solar cells based on SnO₂ electron transport layers.



Faming Li received his Ph.D. degree from Nanjing University in 2016. He is currently an associate professor at School of Materials and Energy, University of Electronic Science and Technology of China. His research focuses on perovskite solar cells.



Mingzhen Liu obtained her master's degree from University of Cambridge. Later, she received her Ph.D. degree from University of Oxford. In 2016, she joined University of Electronic Science and Technology of China and now she serves as a professor and vice dean of School of Materials and Energy. Her research focuses on perovskite materials and solar cell devices.